Magnetic Davydov Splittings in the Optical Absorption Spectrum of Cr_2O_3†

J. W. ALLEN*
Department of Electrical Engineering, Stanford University, Stanford, California 94305
R. M. MACFARLANE‡
Department of Physics, Stanford University, Stanford, California 94305
AND
R. L. WHITE
Department of Electrical Engineering, Stanford University, Stanford, California 94305
(Received 12 September 1968; revised manuscript received 27 November 1968)

Five sharp lines in the optical absorption spectrum of antiferromagnetic Cr_2O_3 are investigated, and the assignments of four of the lines as Frenkel exciton absorptions are discussed in detail. A previous exciton assignment of these lines is shown to be inconsistent with the results of a detailed group-theory analysis of the manner in which interion interactions govern the spectrum, and of the effect of an externally applied magnetic field. All difficulties of the previous assignment are removed by new assignments in which the lines are pairs of Davydov-split Frenkel excitons and none of the energy separations in the spectrum are single-ion exchange splittings. The Davydov splittings are very large, and the mechanism for the large splittings is found, in a first-principles treatment of the interion interactions, to be interion exchange. This result is not predicted by the usually assumed, phenomenological, total-spin Heisenberg exchange interaction, which is an inadequate representation of the exchange interaction between two ions in states of different total spin. New experimental data on the circular polarizations of the split components of the lines in an axial Zeeman experiment, and on the temperature dependence of the positions of the lines, confirm the new assignments. In addition, new data on the temperature dependence of the integrated intensities of the lines and on their stress dependence are presented. The assignment of the fifth line as a magnon sideband is discussed briefly.

I. INTRODUCTION

CHROMIUM oxide is an antiferromagnetic insulator with a Néel temperature of 308°K.[1] The crystal structure is corundum and the chromiums and oxygens bond to produce a Cr^{3+} ion with spin $\frac{3}{2}$. The chromium spins, four per trigonal unit cell, lie along the crystal c axis and alternate up and down, the magnetic space group being $R\bar{3}'c'$.[1] Because the Cr^{3+} ion has sharp optical absorption lines, notably the transitions between the $^4A_2$ ground state and ^2E excited levels (the same transitions used in the ruby laser), and because interion chromium interactions are strong, as evidenced by the high Néel temperature, Cr_2O_3 is a prime candidate for observing optically the effects of exchange and thereby extracting information about the interion couplings in the material.

The optical absorption spectrum of Cr_2O_3 greatly resembles the single-ion (crystal field) spectrum of the Cr^{3+} ion in Al_2O_3 (ruby).[2] In particular, there are several reasonably sharp lines in the red and these are associated with single-ion transitions between the $^4A_2$ and ^2E crystal-field levels. The basic unpolarized spectrum is shown in the left-hand trace of Fig. 1. There are five lines labeled 1–5, and on the basis of their polarizations, which are also given in the figure, lines 1–4 may be distinguished from line 5. Lines 1–4 are electric dipole, there beinq two σ and two π polarized lines with only the σ lines being observed in an axial spectrum. Line 5 is observed in σ and π, but not axial polarization, implying a mixed electric and magnetic dipole character. The positions of lines 1–5 as measured

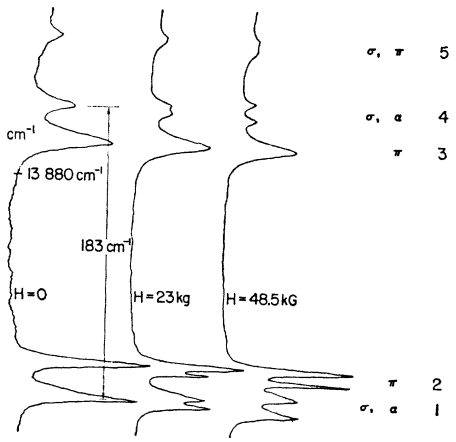

FIG. 1. Zeeman effect in unpolarized absorption spectrum of $^4A_2 \rightarrow {}^2E$ excitons in Cr_2O_3. Polarizations and labeling are given in right-hand columns.

† Based upon a Ph.D. thesis by J. W. Allen, Stanford University, 1968; supported in part by the National Science Foundation under Grant No. GK1646, and in part by the U. S. Army Research Office (Durham). Various technical services were supplied by the Advanced Research Projects Agency through the Center for Materials Research at Stanford University.
* Present address: Lincoln Laboratory, Massachusetts Institute of Technology, Lexington, Mass.
‡ Present address: IBM Research Laboratory, San Jose, Calif.
[1] J. P. van der Ziel, Phys. Rev. Letters 18, 237 (1967). This reference gives original references for the properties of Cr_2O_3.
[2] D. S. McClure, J. Chem. Phys. 38, 2289 (1963).

by Wickersheim[3] and confirmed in the present study are, respectively, 13 743.3, 13 764.1, 13 903.4, 13 926.3, and 13 970.5 cm^{-1} referred to vacuum. This paper is concerned principally with the $T=0°K$ assignment of lines 1–4.

The site symmetry of the Cr^{3+} ion is C_3, so that, including spin-orbit coupling, the ^2E and $^4A_2$ levels of the cubic approximation each split into four levels labeled by the irreducible double group representations of C_3. If time reversal were a site symmetry operation, as it is for the Cr^{3+} ion in Al_2O_3, then each set of four levels would consist of two Kramers doublets, but this does not happen in Cr_2O_3 because the magnetic ordering prevents time reversal from being a site symmetry operation. Splittings of crystal-field levels due to the absence of time-reversal symmetry in a magnetically ordered material are usually called exchange splittings.

The resulting situation in Cr_2O_3 is shown in Fig. 2. The single-ion energy levels are labeled by C_3 double group representations[4] and an up or down arrow that indicates the sign of the z component of spin angular momentum associated with the state. Strictly, the symbol $\uparrow$ or $\downarrow$ is not a proper label, but for the particular Cr^{3+} ion states considered here the orbital angular momentum is nearly zero, leaving the spin angular momentum an almost good quantum number. It may be noted that the spin character of the a_4 and a_5 ground and excited states is reversed. This labeling is correct and is related to the negative g value of the ^2E a_4, a_5 Kramers doublet, as discussed by Clogston[5] and by others. Also shown in Fig. 2 are the polarizations predicted from group theory for electric-dipole transitions to the four upper levels from the lowest ground-state

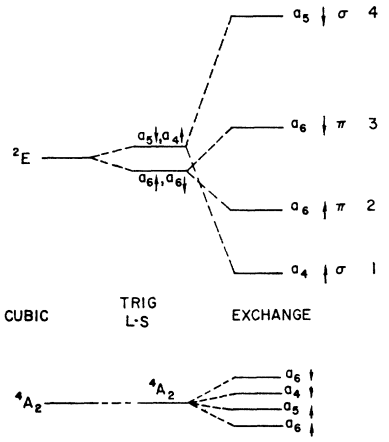

FIG. 2. Exchange-split ^2E and $^4A_2$ Cr^{3+} single-ion energy levels. Polarizations predicted for four $^4A_2$ $a_6\uparrow \rightarrow {}^2E$ electric dipole absorptions and Wickersheim's assignments are given at the right.

level and the assignments for lines 1–4 made by Wickersheim[3] on the basis of their observed polarizations. This assignment encountered the difficulty that although transitions from the lowest ground-state level to the highest two excited states are not forbidden by symmetry, the single-ion mechanisms leading to an electric-dipole moment are too small to make these transitions observable, as is experimentally verified by Zeeman studies of the Cr^{3+} ion in ruby.[6]

The behavior of the spectrum when a magnetic field is applied to the sample was observed by Stager,[7] and more recently by van der Ziel.[8] There is no response if the field is applied perpendicular to the c axis, but for the field parallel to the c axis, the spectrum changes as shown in Fig. 1, which presents data confirming previous work. Lines 1 and 4 split uniformly with splitting factors that are equal within experimental error, van der Ziel's values being 4.62 and 4.66, respectively. Line 3 is unaffected by the field and line 2 develops a π-polarized satellite, which will be referred to as 2′. As the field increases, the intensity of 2′ increases and 2 and 2′ shift to increase their separation. If the separation is extrapolated to zero field, where 2′ is unobservable, it is found that a zero-field separation of 3.75 cm^{-1} exists.

Stager assigned g values to the single-ion Kramers doublets and tried to interpret the magnetic splittings in terms of Wickersheim's assignments as arising from the magnetic-field-induced inequivalence of up- and down-spin sites. Using this model, an internally consistent assignment of g values could not be found, and the qualitative behavior of lines 2 and 2′, first observed carefully by van der Ziel, could not be understood. Van der Ziel showed that the qualitative behavior of lines 2 and 2′ could be explained if the lines were assigned as transitions from the ground state to $\mathbf{k}=0$ Frenkel exciton states. Treatment of the excited states of magnetic insulators as excitons allows for the effects of interion couplings in delocalizing an excitation, and was first suggested by Loudon[9] in a recently published paper which was widely circulated prior to publication. As will be discussed in Sec. II each single-ion transition gives rise to a $\mathbf{k}=0$ exciton state, and each $\mathbf{k}=0$ exciton state has associated with it a multiplicity of four because Cr_2O_3 has four Cr^{3+} ions per unit cell. The distribution of the multiplicity, i.e., a quartet, two doublets, etc., is determined by the symmetry of the unit cell, departures from a quartet being called Davydov splittings. In particular there is a well-known procedure, which will be reviewed in Sec. II, for classifying the $\mathbf{k}=0$ states arising from some single-ion transition according to irreducible representations of the crystal's factor group, which describes the symmetry of the unit cell. For a magnetic crystal, the factor

[3] K. A. Wickersheim, J. Appl. Phys. **34**, 1224 (1963).
[4] The representations are labeled so that the character of counterclockwise C_3 in a_1–a_6 is 1, $e^{2i\pi/3}$, $e^{-2i\pi/3}$, $e^{i\pi/3}$, $e^{-i\pi/3}$, and -1, respectively.
[5] A. M. Clogston, Phys. Rev. **118**, 1229 (1960).
[6] M. D. Sturge (private communication).
[7] C. V. Stager, J. Appl. Phys. **34**, 1232 (1963).
[8] J. P. van der Ziel, Phys. Rev. **161**, 483 (1967).
[9] R. Loudon, Advan. Phys. **17**, 243 (1968).

group may contain antiunitary operators and the classification is usually done using the factor group's unitary subgroup, whose representations are inspected for extra degeneracy due to the antiunitary operators as discussed by Dimmock and Wheeler[10] and using the test developed by them. Lax[11] has shown that selection rules determined using these unitary representation labels are valid when the initial and final states of a transition are not connected by one of the antiunitary operators, a condition satisfied for the transitions being discussed here. The result of applying the classification procedure for single-ion transitions from the lowest exchange-split ground state to the four exchange-split excited levels of the Cr^{3+} ion in Cr_2O_3 is shown in Fig. 3, including the predicted electric-dipole selection rules and van der Ziel's assignment of lines 1–4. It can be shown from group theory that a magnetic field applied parallel to the crystal c axis may split the E levels and couple the A_1 and A_2 levels. Thus line 2′ can be assigned as an unobservable transition between the ground state and a Davydov-split A_1 level, which by mixing with line 2 becomes observable when the magnetic field is applied. The insensitivity of line 3 to field was explained by assuming its magnetic-field coupling to any A_1 levels was very small. Van der Ziel did not attempt to explain the observed magnitudes of the magnetic splitting or coupling factors.

There are three difficulties with van der Ziel's assignment. The first is that the number of lines predicted is twice the number observed. Van der Ziel has attempted to explain this by invoking the group appropriate to the paramagnetic state as an approximate symmetry group.

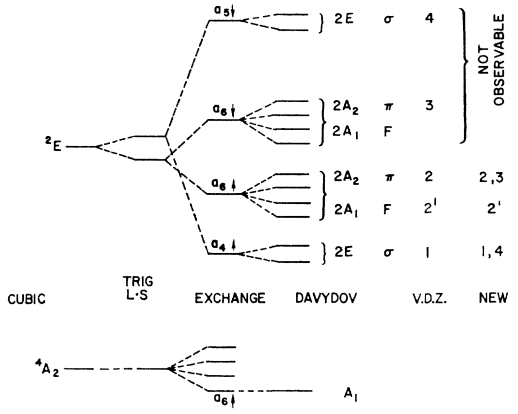

FIG. 3. Davydov-split $\mathbf{k}=0$ exciton states in Cr_2O_3. Electric-dipole selection rules (F means forbidden), van der Ziel's (V.D.Z.) assignments, and the new assignments as they appear with V.D.Z. ordering of energy levels are shown at right.

The paramagnetic group contains inversion and the previous results are altered in that representations labeling the states appear in pairs with odd and even parity, thus making electric-dipole transitions to half the levels forbidden. As will be discussed carefully in Sec. II, this is an incorrect application of the approximate symmetry concept, essentially because the states used to describe the exciton levels do not form, even approximately, a basis for a representation of the paramagnetic group. The second difficulty is the same one encountered previously by Wickersheim. Because transitions to Frenkel exciton states derive all their intensity from single-ion processes[12] it is not possible to account for the observed intensities of lines 3 and 4. Van der Ziel postulated that interion exchange interactions might provide an effective single-ion mechanism of sufficient size to account for the transitions. A generalization which includes this idea is to observe that there may be matrix elements of the interion interactions between exciton states of the upper levels and exciton states of the lower levels if both states belong to the same representation of the factor group. In Sec. III, where a first-principles analysis of the interactions is given, it will be seen that such matrix elements are not of sufficient size to explain the intensities of lines 3 and 4. The last difficulty is in explaining the magnitudes of the magnetic splitting and coupling factors, and the observed circular polarization properties of lines 1 and 4 in an axial Zeeman experiment. The magnetic splitting and coupling factors, including their signs, which determine the circular polarization properties, can be related to single-ion g values, as will be shown in Sec. II, and an internally consistent fit with the data is impossible using van der Ziel's assignments.

All these difficulties arise from assigning lines 3 and 4 as transitions to levels arising from the upper single-ion excited states, and may be avoided if lines 1–4 are identified as allowed electric-dipole transitions to the Davydov-split levels arising from the lower two single-ion excited states only. Evidently there is no longer any need to give an intensity mechanism for the upper two levels; the number of lines predicted becomes the number observed, and it will be shown that the magnetic coupling and splitting factors can be understood quantitatively.

The principal issue raised by the new assignment is that Davydov splittings in the optical spectrum of magnetic insulators have previously been estimated to be of the order of a few cm^{-1} at most,[8] while Fig. 1 shows that the splittings identified here are as large as 180 cm^{-1}. This point is emphasized by Fig. 3, which shows the new assignments as they appear with van der Ziel's ordering of the energy levels, where the Davydov splittings are fine structure rather than major features. To know whether this is a reasonable result requires a detailed knowledge of how the interion couplings deter-

[10] J. O. Dimmock and R. G. Wheeler, in *The Mathematics of Physics and Chemistry*, edited by H. Margenau and G. M. Murphy (D. Van Nostrand, Inc., Princeton, N. J., 1964), Vol. 2, Chap. 12.

[11] M. Lax, in *Proceedings of the International Conference on the Physics of Semiconductors, Exeter, 1962* (The Institute of Physics and the Physical Society, London, 1962).

[12] A. S. Davydov, *Theory of Molecular Excitons* (McGraw-Hill Book Co., New York, 1962).

mine the spectrum. The group-theory analysis in Sec. II obtains the Davydov splitting patterns in terms of specific interion couplings, and Sec. III discusses the mechanisms responsible for these couplings. By making a first-principles analysis of exchange that goes beyond the total-spin Heisenberg interion interaction usually assumed, it is possible to show that the large splitting is due to energy transfer via the exchange interaction between ions whose spins in the ground-state configuration are aligned.

In Sec. IV, new experimental data on the temperature, stress, and magnetic-field dependence of the lines are presented and discussed in terms of the reassignment proposed here.

II. GROUP-THEORY ANALYSIS OF OPTICAL EXCITONS

With the work of Loudon,[9] it is now generally accepted that the excited states of a magnetic insulator are best described as Frenkel excitons. The formalism is appropriate not only for the optical levels to be discussed here, but also for the low-lying excitations, which are usually called spin waves. The Frenkel exciton states result from diagonalization of the crystal Hamiltonian in a certain subspace of states, to be specified below. Labeling the ion sites by $\mathbf{R}_{ni}$, a vector specifying the location of the ith of p ions in the nth of N unit cells, the crystal Hamiltonian can be written

$$\mathcal{H}=\sum_{i=1}^{p}\sum_{n=1}^{N}\mathcal{H}(\mathbf{R}_{ni})+\sum_{\mathbf{R}_{ni}\neq\mathbf{R}_{mj}}\mathcal{H}(\mathbf{R}_{ni},\mathbf{R}_{mj}). \quad (2.1)$$

$\mathcal{H}(\mathbf{R}_{ni})$ is the single-ion crystal-field Hamiltonian and contains the usual phenomenological crystal electric-field terms, spin-orbit coupling, and Coulomb interactions between the magnetic shell electrons on the ion. It is independent of i and n except for the over-all rotational orientation of the crystal electric-field terms. The eigenstates of $\mathcal{H}(\mathbf{R}_{ni})$ can be combined to specify a state of the crystal by giving the state of each ion, and the antisymmetrized product of the functions associated with the single-ion states defines what will be called a crystal state, denoted by

$$|\mu\mathbf{R}_{01},\mu\mathbf{R}_{02},\cdots,\mu\mathbf{R}_{ni},\cdots,\mu\mathbf{R}_{Np}\rangle, \quad (2.2)$$

where μ is a collective index giving all pertinent quantum numbers of the crystal-field state and will include the row of some representation of the site group. The crystal state with the lowest-energy diagonal matrix element of $\mathcal{H}$ will be called the ground-state spin arrangement $|G\rangle$, which in Cr_2O_3 is

$$|G\rangle=|{}^4A_2+\tfrac{3}{2},{}^4A_2-\tfrac{3}{2},{}^4A_2+\tfrac{3}{2},{}^4A_2-\tfrac{3}{2},\cdots\rangle. \quad (2.3)$$

Note that the single-ion terms of $\mathcal{H}$ determine the lowest-energy crystal-field state and the interion terms of $\mathcal{H}$ determine the lowest-energy relative spin arrangement of the ions. The departure of $|G\rangle$ from being an exact eigenstate of the full Hamiltonian does not seriously affect the results of this discussion, which tacitly assumes $|G\rangle$ to be an eigenstate. Denote by $|\mu\mathbf{R}_{ni}\rangle$ a crystal state that differs from $|G\rangle$ in that the ion at $\mathbf{R}_{ni}$ has a state μ different from its state in $|G\rangle$. Again the interion terms of $\mathcal{H}$ will distinguish energetically among the possible choices of the z component of the angular momentum of state μ, inducing diagonal energy differences which are the exchange splittings mentioned in Sec. I and are shown schematically on a single-ion energy-level diagram like that in Fig. 2 for Cr_2O_3.

The magnetic space group $\mathcal{G}$ of a crystal can be defined as the set of operations that leave $|G\rangle$ invariant. Consider operating with an element Θ of $\mathcal{G}$ on a state $|\mu\mathbf{R}_{ni}\rangle$, presuming μ to be a one-dimensional representation of the site group, as would be the case in Cr_2O_3. If Θ maps $\mathbf{R}_{ni}$ into $\mathbf{R}_{mj}$, then

$$\Theta|\mu\mathbf{R}_{ni}\rangle=e^{i\varphi}|\nu\mathbf{R}_{mj}\rangle, \quad (2.4)$$

where $\nu=\mu$ if $\mathbf{R}_{ni}$ and $\mathbf{R}_{mj}$ have the same spin in $|G\rangle$ and $\nu=\mu^*$, the representation related to μ by the time reversal, if $\mathbf{R}_{ni}$ and $\mathbf{R}_{mj}$ have opposite spins in $|G\rangle$. That $\nu=\mu^*$ in the latter case follows because Θ leaves $|G\rangle$ invariant. By letting Θ run over the elements of $|G\rangle$, $p.N$ states are generated, each representing the excitation of a different one of the $p.N$ ions, and each having the same on-diagonal matrix element of $\mathcal{H}$. This follows by observing that, since $[\mathcal{G},\mathcal{H}]=0$,

$$\langle\mu\mathbf{R}_{ni}|\mathcal{H}|\mu\mathbf{R}_{ni}\rangle=\langle\Theta\mu\mathbf{R}_{ni}|\,\Theta\mathcal{H}\Theta^{-1}|\,\Theta\mu\mathbf{R}_{ni}\rangle$$
$$=\langle\nu\mathbf{R}_{mj}|\mathcal{H}|\nu\mathbf{R}_{mj}\rangle. \quad (2.5)$$

This result also implies that all the ions have the same set of exchange-split energy levels, taking into account that the same energy levels on opposite spin ions are labeled by time-reversal related site-group representations. The off-diagonal matrix elements of $\mathcal{H}$ will couple the $p.N$ crystal states among themselves and these matrix elements are frequently called transfer-of-excitation matrix elements. Diagonalization of $\mathcal{H}$ in this $p.N$-dimensional subspace, where all the states are physically equivalent and have equal on-diagonal matrix elements, results in the Frenkel excitons. Choosing μ in the single-ion ground-state spin manifold gives magnons, and choosing μ in a higher-lying single-ion manifold gives optical excitons.

Diagonalization of $\mathcal{H}$ in this subspace is rendered possible by observing that because of the way the pN states were generated, they form a basis for a $p.N$-dimensional representation of $\mathcal{G}$. Because $[\mathcal{G},\mathcal{H}]=0$ the linear combinations of these states that reduce this representation into irreducible representations of $\mathcal{G}$ will diagonalize $\mathcal{H}$ except for the possiblity of matrix elements between linear combinations belonging to the same irreducible representation. Now it is true that the first-principles crystal Hamiltonian is invariant to a larger group of operators than $\mathcal{G}$; for example, it is

certainly time-reversal-invariant. As Anderson[13] has discussed, $|G\rangle$, which defines $\mathcal{G}$, should be regarded as a broken symmetry state of $\mathcal{H}$, that is, it is left invariant by only a subgroup of the full group of $\mathcal{H}$. It is clear, however, that if $\mathcal{H}$ is to be diagonalized not in a complete set of states, but in a subset like the set of pN states considered here, the relevant symmetry group is the largest subgroup of the full group of $\mathcal{H}$ for which the subset of states forms a basis for a representation, the subgroup in this case being $\mathcal{G}$. From this point of view it is clear that introducing the paramagnetic group, as van der Ziel has done for Cr_2O_3, is only appropriate when the interion terms in $\mathcal{H}$ produce negligible single-ion exchange splittings. van der Ziel's assignments assume sizeable single-ion exchange splittings, which is undoubtedly the case in Cr_2O_3, but is inconsistent with his use of the paramagnetic group as an approximate symmetry group.

A partial reduction of the representation and a corresponding partial diagonalization of the Hamiltonian matrix is accomplished by making linear combinations of the $|\mu\mathbf{R}_{ni}\rangle$ which will transform irreducibly in the translation subgroup T of $\mathcal{G}$. These linear combinations are well known to be given by

$$|\mathbf{k}i\rangle = N^{-1/2}\sum_n e^{-i\mathbf{k}\cdot\mathbf{T}_n}|\mathbf{R}_{ni}\rangle, \qquad (2.6)$$

where $\mathbf{T}_n$ is the pure lattice translation that takes unit cell $n=0$ into unit cell n. Since all the states being considered, including $|\mathbf{k}i\rangle$, are labeled by μ or μ^*, this subscript has been suppressed. After this transformation, the Hamiltonian matrix will block down into N blocks, each of dimension p, each labeled by a $\mathbf{k}$ vector, and each having equal on-diagonal matrix elements. This is evident from group theory, or it can easily be shown directly that

$$\langle\mathbf{k}i|\mathcal{H}|\mathbf{k}'j\rangle = \delta_{\mathbf{k}\mathbf{k}'}\sum_{\mathbf{T}_{nm}} e^{-i\mathbf{k}\cdot\mathbf{T}_{nm}}H(\mathbf{T}_{nm}+\boldsymbol{\tau}_{ij}), \qquad (2.7)$$

where

$$H(\mathbf{T}_{nm}+\boldsymbol{\tau}_{ij}) \equiv \langle\mathbf{R}_{ni}|\mathcal{H}|\mathbf{R}_{mj}\rangle,$$
$$\mathbf{T}_{nm} \equiv \mathbf{T}_m - \mathbf{T}_n = \mathbf{R}_{mj} - \mathbf{R}_{nj},$$
$$\boldsymbol{\tau}_{ij} \equiv \mathbf{R}_{nj} - \mathbf{R}_{ni}.$$

What remains is to diagonalize each subblock. This is aided by realizing that the $|\mathbf{k}i\rangle$ must be a basis for a representation of the factor group $\mathcal{G}_\mathbf{k}/T$, where T is the translation subgroup and $\mathcal{G}_\mathbf{k}$ is the (magnetic) group of the $\mathbf{k}$ vector, since the linear combinations of $|\mathbf{k}i\rangle$ that reduce this representation will be part of a basis for an irreducible representation of $\mathcal{G}$. The generators of the factor group themselves may be regarded as a group that leaves invariant a unit cell (say, $n=0$) with periodic boundary conditions, and this is a convenient viewpoint since then the $|\mathbf{k}i\rangle$ may be temporarily replaced by the $|\mathbf{R}_{0i}\rangle$ in performing the group-theory analysis. Since $\mathbf{k}$ will remain a good quantum number, and since the $\mathbf{k}\approx 0$ photons will only excite $\mathbf{k}\approx 0$ excitons, the analysis will be done for Cr_2O_3 only for the $\mathbf{k}=0$ subblock. The generators of the factor group of $\mathcal{G}_{\mathbf{k}=0}$ form the full covering group of a periodic unit cell, which is usually called *the* factor group of the crystal. For Cr_2O_3, $p=4$, and the (magnetic) factor group operations are $\{E,0\}$, $2\{C_3|0\}$, $3\{C_2|0\}$, $\{RI|0\}$, $2\{RIC_3|0\}$, $3\{RIC_2|\tau\}$, and products with $\{\bar{E}|0\}$ to obtain the double group. R is the time-reversal operator and τ is a translation along the C_3 axis by half the length of the unit cell along that axis. These operations are isomorphic to the magnetic point group, in the Schoenflies notation, $D_{3d}(D_3)$. Figure 4 shows schematically the trigonal unit cell, the ground-state spin arrangement of the four C_3-axis ions, and the locations of the inversion centers and the C_2 axes. The unit-cell ions are labeled 1–4 and their single-ion states are listed in that order in a crystal-state ket.

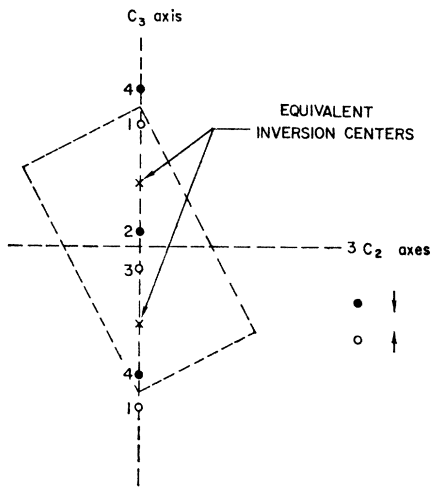

FIG. 4. Schematic trigonal unit cell for Cr_2O_3 showing symmetry operations and labeling of unit-cell ions.

The single-ion exchange-split energy levels for the four ions are shown in Fig. 5, using labels for the group

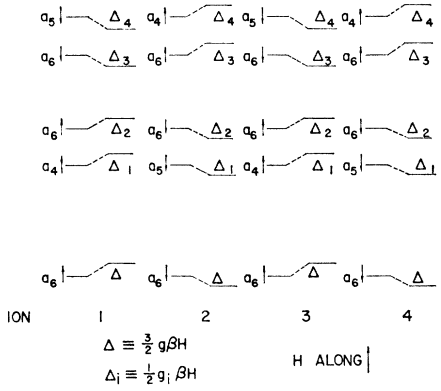

FIG. 5. Exchange-split single-ion energy levels for four unit-cell ions and effect of applied magnetic field on energy levels.

[13] P. W. Anderson, *Concepts In Solids* (W. A. Benjamin, Inc., New York, 1964).

C_3 with spin-orbit coupling. With these labels, $|G\rangle$ is given by

$$|G\rangle = |a_6\uparrow, a_6\downarrow, a_6\uparrow, a_6\downarrow, \cdots\rangle. \tag{2.8}$$

The set of four $|\mathbf{R}_{0i}\rangle$ functions describing the excitation of a single ion to the lowest excited level of Fig. 5 will be designated Γ_1 and are given by

$$\begin{aligned} |1\rangle &= |ea_4\uparrow, ga_6\downarrow, ga_6\uparrow, ga_6\downarrow\rangle, \\ |2\rangle &= |ga_6\uparrow, ea_5\downarrow, ga_6\uparrow, ga_6\downarrow\rangle, \\ |3\rangle &= |ga_6\uparrow, ga_6\downarrow, ea_4\uparrow, ga_6\downarrow\rangle, \\ |4\rangle &= |ga_6\uparrow, ga_6\downarrow, ga_6\uparrow, ea_5\downarrow\rangle, \end{aligned} \tag{2.9a}$$

where only the pertinent index i has been retained, and g and e refer to ground and excited states, respectively. The four states differ only in which ion is excited. The rest of the lattice's ions, all in their ground states, are omitted because this combination transforms identically and contributes nothing to the analysis. For transitions to the next highest excited level of Fig. 5, the four $|\mathbf{R}_{0i}\rangle$, denoted as Γ_2, are

$$\begin{aligned} |1\rangle &= |ea_6\uparrow, ga_6\downarrow, ga_6\uparrow, ga_6\downarrow\rangle, \\ |2\rangle &= |ga_6\uparrow, ea_6\downarrow, ga_6\uparrow, ga_6\downarrow\rangle, \\ |3\rangle &= |ga_6\uparrow, ga_6\downarrow, ea_6\uparrow, ga_6\downarrow\rangle, \\ |4\rangle &= |ga_6\uparrow, ga_6\downarrow, ga_6\uparrow, ea_6\downarrow\rangle. \end{aligned} \tag{2.9b}$$

For the remaining two excited states the sets of functions are similar and will be denoted Γ_3 and Γ_4, Γ_4 belonging to the highest level shown in Fig. 5.

Because the magnetic-factor group is an antiunitary group, the representation generated by each Γ_n should be called a corepresentation, in Wigner's terminology,[14] and following him, the first step in reducing a corepresentation is to reduce it into the unitary subgroup of the antiunitary group, which in this case is D_3. The representations of D_3 that will appear are rather easily found, since the character of the reducible representation Γ_n is given by the formula

$$\begin{aligned} \chi(\Theta) &= \sum_{i=1}^{4} \chi_i^{s\cdot g\cdot}(\Theta), \quad \Theta \text{ in the site group} \\ &= 0, \qquad\qquad\quad \Theta \text{ not in the site group} \end{aligned} \tag{2.10}$$

where $\chi_i^{s\cdot g\cdot}(\Theta)$ is the character of the site-group representation for which $|\mathbf{R}_{0i}\rangle$ is a basis. This result follows from observing that only site-group operations do not permute the functions, and hence will have diagonal elements in their representation matrices. The transformation properties of an $|\mathbf{R}_{0i}\rangle$ are found by transforming each single-ion component separately. Applying Eq. (2.10) for each set of functions Γ_n, and then reducing the representation with respect to D_3 yields the unitary subgroup $\mathbf{k}=0$ exciton labels

$$\begin{aligned} &\Gamma_1 \to 2E, \qquad &&\Gamma_3 \to 2A_1+2A_2, \\ &\Gamma_2 \to 2A_1+2A_2, \qquad &&\Gamma_4 \to 2E. \end{aligned}$$

This is the result obtained by van der Ziel and shown in Fig. 3. The Dimmock-Wheeler test for extra degeneracy due to the group's antiunitary operators shows that the dimensions of these representations are unaffected. Also, since the component of the magnetic-dipole operator along the C_3 axis, μ_z, transforms as A_2 in D_3, it is easy to work out that a magnetic field applied along the C_3 axis can cause matrix elements only between two E states or between an A_1 and an A_2 state. By the Lax[11] theorem, the antiunitary operators will not change this result.

Knowing the representations of D_3 that appear for a particular Γ_n, projection operators[15] for these representations can be used to find the linear combinations of $|\mathbf{R}_{0i}\rangle$ (and hence $|\mathbf{k}=0, i\rangle$) that transform irreducibly in the unitary subgroup. The only subtlety in carrying this out is to observe that from the group multiplication table $C_2''=C_3C_2'$ and $C_2'''=C_3^{-1}C_2'$, so that phase factors from the site-group representations enter the transformation for two of the C_2 operations. This reflects the fact that the oxygens surrounding two sites interchanged by the $3C_2$'s are mapped differently by the different C_2 operations. The coefficients of the resulting linear combinations define the columns of a transformation matrix S such that $S^\dagger \mathcal{H} S \equiv \tilde{\mathcal{H}}$ must have a form consistent with the group-theory matrix-element theorem. Requiring this form to appear, and using the known fact that all the H_{ii} are equal, yields restrictions on the six matrix elements $H_{ij} \equiv \langle \mathbf{k}=0, i|\mathcal{H}|\mathbf{k}=0, j\rangle$. For Γ_1 and Γ_4 these restrictions are found to be $H_{12}=H_{34}=H_{14}=H_{23}=0$ and $H_{13}=H_{42}$. For Γ_2 and Γ_3 the restrictions are $H_{13}=H_{42}$, $H_{12}=H_{43}$, and H_{23} and H_{14} real. Doublets arise for the Γ_1 and Γ_4 functions because of the restrictions that all the H_{ij} except $H_{13}=H_{42}$ are zero, and these restrictions are directly traceable to the fact that for all the H_{ij} except $H_{13}=H_{42}$ the excitation must transfer between sublattices whose equal-energy excited states transform differently in the site group, being Kramers pairs a_4 and a_5. This situation is peculiar to a magnetic crysta and the observation of true doublets in the spectrum is quite a detailed confirmation of the model. The lack of similar restrictions for Γ_2 and Γ_3 comes because Kramers pairs $a_6\uparrow$ and $a_6\downarrow$ transform the same in the site group. The observation of singlets in the spectrum is again good confirmation of the model.

The effect of a magnetic field applied parallel to the c axis is included by assigning parallel g values g and g_l, $l=1$ to 4, to the single-ion ground and excited states, respectively, and then computing the changes that the field induces in the H_{ii}. The changes of the single-ion

[14] E. P. Wigner, *Group Theory* (Academic Press Inc., New York, 1959).

[15] M. Tinkham, *Group Theory and Quantum Mechanics* (McGraw-Hill Book Co., New York, 1964).

energies for a field parallel to the ground-state spin on ion 1 are shown in Fig. 5 and the changes may be taken as definitions of g and the g_l. With no excited-state mixings of the type proposed by van der Ziel, $g_1=g_4$ and $g_2=g_3$. To obtain the new H_{ii} the changes in energy for each component of $|R_{0i}\rangle$ are added up, giving, for $l=1$ and 2,

$$\begin{aligned} H_{11}(\Gamma_l)&=E_l+\tfrac{1}{2}g_l\beta H-\tfrac{3}{2}g\beta H+\tfrac{3}{2}g\beta H-\tfrac{3}{2}g\beta H \\ &=E_l+\tfrac{1}{2}\beta H(g_l-3g), \\ H_{22}(\Gamma_l)&=E_l-\tfrac{1}{2}\beta H(g_l-3g), \\ H_{33}(\Gamma_l)&=E_l+\tfrac{1}{2}gH(g_l-3g), \\ H_{44}(\Gamma_l)&=E_l-\tfrac{1}{2}\beta H(g_l-3g). \end{aligned} \tag{2.11}$$

For $l=3$ and 4 all plus and minus signs except on E_l are reversed. This procedure may seem somewhat phenomenological, but it corresponds to solving the crystal-field problem in the presence of the magnetic field, obtaining the g values, and then ignoring small field-induced changes in the $H=0$ wave functions, which would cause small changes in the off-diagonal H_{ij}. Also ignored are direct couplings by the magnetic field of states on different ions. This last approximation is expected to be good on the empirical grounds that the observed insensitivity of the Cr_2O_3 lines to a magnetic field applied perpendicular to the c axis is easily explained as due to the known negligibly small perpendicular g values of the single-ion levels in ruby.

Because the applied field lowers the symmetry and prevents all the H_{ii} from being equal, certain of the elements of $\tilde{\mathcal{H}}$, which are zero by symmetry for no applied field, become nonzero in the presence of the field. Using Eq. (2.11) and the restrictions mentioned above for the off-diagonal H_{ij}, the $\Gamma_1 S^\dagger \tilde{\mathcal{H}} S \equiv \tilde{\mathcal{H}}(\Gamma_1)$ has the form, including the magnetic field,

$$\begin{aligned} \tilde{\mathcal{H}}(\Gamma_1)&=\tfrac{1}{2}\begin{bmatrix}1&0&0&1\\0&1&1&0\\i&0&0&-i\\0&-i&i&0\end{bmatrix}\begin{bmatrix}H_{11}&H_{12}&H_{13}&H_{14}\\H_{12}^*&H_{22}&H_{23}&H_{24}\\H_{13}^*&H_{23}^*&H_{33}&H_{34}\\H_{14}^*&H_{24}^*&H_{34}^*&H_{44}\end{bmatrix}\begin{bmatrix}1&0&-i&0\\0&1&0&i\\0&1&0&-i\\1&0&i&0\end{bmatrix} \\ &\qquad |x_1E\rangle \qquad |x_2E\rangle \qquad |y_1E\rangle \qquad |y_2E\rangle \\ &=\begin{bmatrix}E&H_{13}&+\tfrac{1}{2}i\beta H(3g-g_1)&0\\H_{13}^*&E&0&+\tfrac{1}{2}i\beta H(3g-g_1)\\-\tfrac{1}{2}i\beta H(3g-g_1)&0&E&H_{13}^*\\0&-\tfrac{1}{2}i\beta H(3g-g_1)&H_{13}^*&E\end{bmatrix}, \end{aligned} \tag{2.12}$$

where x and y label, respectively, the first and second rows of E, since that is how the rows transform, and the subscripts on the x and y labels distinguish the two E representations. For Γ_2, the transformation matrix S and $\tilde{\mathcal{H}}(\Gamma_2)=S^\dagger\tilde{\mathcal{H}}S$ is given by

$$S=\frac{1}{\sqrt{2}}\begin{bmatrix}1&0&1&0\\0&1&0&1\\0&1&0&-1\\1&0&-1&0\end{bmatrix} \tag{2.13a}$$

and

$$\begin{aligned} \tilde{\mathcal{H}}(\Gamma_2)&= \\ &\begin{array}{c} \quad |IA_1\rangle \qquad\quad |IIA_1\rangle \qquad\quad |IA_2\rangle \qquad\quad |IIA_2\rangle \\ \begin{bmatrix}E+H_{14}&R_1e^{i\varphi_1}&\tfrac{1}{2}(g_2-3g)\beta H&0\\R_1e^{-i\varphi_1}&E+H_{23}&0&-\tfrac{1}{2}(g_2-3g)\beta H\\\tfrac{1}{2}(g_2-3g)\beta H&0&E-H_{14}&R_2e^{i\varphi_2}\\0&-\tfrac{1}{2}(g_2-3g)\beta H&R_2e^{-i\varphi_2}&E-H_{23}\end{bmatrix}\end{array}, \end{aligned} \tag{2.13b}$$

where

$$R_1e^{i\varphi_1}\equiv H_{12}+H_{13}, \qquad R_2e^{i\varphi_2}\equiv H_{12}-H_{13}.$$

Note that the magnetic field matrix elements appear where predicted previously from group theory. Diagonalization of $\tilde{\mathcal{H}}(\Gamma_1)$ for $H=0$ is trivial since for $H=0$, $\tilde{\mathcal{H}}(\Gamma_1)$ is block diagonal with two 2×2 matrices, each having equal on-diagonal elements. But for $\tilde{\mathcal{H}}(\Gamma_2)$, the diagonal blocks for $H=0$ have unequal diagonal elements, so the form of the $H=0$ eigenfunctions appears to depend on the magnitudes of the off-diagonal matrix elements. This difficulty can be removed by considering the effect of the antiunitary operators.

The corepresentation matrices are not yet fully reduced, as will soon be shown. An antiunitary group $A(B)$ may be decomposed as[15]

$$A(B)=B+\Theta_0B,$$

where B is the unitary subgroup and Θ_0 is any of the antiunitary operators. Thus it is apparent that if the transformation properties of a set of states are known for B, it sufficies to know how the states transform under Θ_0 to

determine how they transform under any antiunitary element. For $D_{3d}(D_3)$ it is convenient to take $\Theta_0=\{RI|0\}$. It is straightforward to show that the corepresentation matrices for Γ_1 and Γ_2, in the basis for $\tilde{\mathcal{H}}$, have the forms

$$\begin{array}{c} \\ |x_1E\rangle \\ |y_1E\rangle \\ |x_2E\rangle \\ |y_2E\rangle \end{array}\!\!\begin{array}{c} \begin{array}{cccc} |x_1E\rangle & |y_1E\rangle & |x_2E\rangle & |y_2E\rangle \end{array} \\ \left[\begin{array}{cc|cc} \multicolumn{2}{c|}{\multirow{2}{*}{$\Gamma_E(U)$}} & \multicolumn{2}{c}{\multirow{2}{*}{0}} \\ & & & \\ \hline \multicolumn{2}{c|}{\multirow{2}{*}{0}} & \multicolumn{2}{c}{\multirow{2}{*}{$\Gamma_E(U)$}} \\ & & & \end{array}\right] \end{array}, \quad \Gamma_1(RI)=\left[\begin{array}{cc|cc} 0 & & -1 & 0 \\ & & 0 & -1 \\ \hline -1 & 0 & \multicolumn{2}{c}{\multirow{2}{*}{0}} \\ 0 & -1 & & \end{array}\right],$$

$$\Gamma_2(U)=\left[\begin{array}{cc|cc} \chi_{A_1}(U) & 0 & 0 & 0 \\ 0 & \chi_{A_1}(U) & 0 & 0 \\ \hline 0 & 0 & \chi_{A_2}(U) & 0 \\ 0 & 0 & 0 & \chi_{A_2}(U) \end{array}\right], \quad \Gamma_2(RI)=\left[\begin{array}{cc|cc} 0 & 1 & \multicolumn{2}{c}{\multirow{2}{*}{0}} \\ 1 & 0 & & \\ \hline \multicolumn{2}{c|}{\multirow{2}{*}{0}} & 0 & 1 \\ & & 1 & 0 \end{array}\right], \tag{2.14}$$

where U is any of the unitary operators, χ is the character of an irreducible representation, and Γ is an irreducible matrix. These are clearly not in the reduced forms that the Dimmock-Wheeler test shows to be achievable. As Wigner[13] has shown, because the upper-right and lower-left subblocks of the coupled parts of $\Gamma(RI)$ are identical, there exists a transformation that reduces $\Gamma(RI)$ and leaves $\Gamma(U)$ unchanged, and it is the properties of these matrices as determined by the nature of A_1, A_2, and E, and the structure of $D_{3d}(D_3)$, that enters the Dimmock-Wheeler test. The unitary transformations S_1 and S_2 that reduce $\Gamma_1(RI)$ and $\Gamma_2(RI)$, respectively, are given by

$$\sqrt{2}S_1=\begin{bmatrix} 1 & 0 & e^{i\varphi} & 0 \\ 0 & 1 & 0 & e^{i\varphi} \\ e^{-i\varphi} & 0 & -1 & 0 \\ 0 & e^{-i\varphi} & 0 & -1 \end{bmatrix} \quad \text{and} \quad \sqrt{2}S_2=\left[\begin{array}{cc|cc} 1 & e^{i\theta_1} & \multicolumn{2}{c}{\multirow{2}{*}{0}} \\ e^{-i\theta_1} & -1 & & \\ \hline \multicolumn{2}{c|}{\multirow{2}{*}{0}} & 1 & e^{i\theta_2} \\ & & e^{-i\theta_2} & -1 \end{array}\right], \tag{2.15}$$

where φ, θ_1, and θ_2 are arbitrary. Applying these transformations gives

$$S_1^\dagger\Gamma_1(U)S=\Gamma_1(U), \qquad S_2^\dagger\Gamma_2(U)S=\Gamma_2(U),$$

$$S_1^\dagger\Gamma_1(RI)S_1^*=\left[\begin{array}{cc|cc} e^{i\varphi} & 0 & \multicolumn{2}{c}{\multirow{2}{*}{0}} \\ 0 & e^{i\varphi} & & \\ \hline \multicolumn{2}{c|}{\multirow{2}{*}{0}} & -e^{-i\varphi} & 0 \\ & & 0 & -e^{-i\varphi} \end{array}\right], \quad S_2^\dagger\Gamma_2(RI)S_2^*=\left[\begin{array}{cc|cc} e^{i\theta_1} & 0 & \multicolumn{2}{c}{\multirow{2}{*}{0}} \\ 0 & -e^{-i\theta_1} & & \\ \hline \multicolumn{2}{c|}{\multirow{2}{*}{0}} & e^{-i\theta_2} & 0 \\ & & 0 & -e^{-i\theta_2} \end{array}\right]. \tag{2.16}$$

Note that the use of S_1^* and S_2^* in the last two transformations is correct for an antiunitary operator and that the reduced forms of $\Gamma(U)$ and $\Gamma(RI)$ guarantee a reduced form for the remaining antiunitary operators. Note also that two representations which are indistinguishable with respect to the unitary subgroup may now be distinguished from one another by their transformation properties under RI, and this implies that S_1 and S_2 must diagonalize $\tilde{\mathcal{H}}(\Gamma_1)$ and $\tilde{\mathcal{H}}(\Gamma_2)$, respectively.

If $\tilde{\mathcal{H}}(\Gamma_1)$ is written with the same row ordering used for S_1 and the corepresentation matrices, and φ is chosen as the phase of H_{13}, then

$$\begin{array}{c} \\ |xE^+\rangle \\ |yE^+\rangle \\ |xE^-\rangle \\ |yE^-\rangle \end{array}\!\!\begin{array}{c} \begin{array}{cccc} |xE^+\rangle & |yE^+\rangle & |xE^-\rangle & |yE^-\rangle \end{array} \\ \begin{bmatrix} E+R & +\frac{1}{2}i(3g-g_1)\beta H & 0 & 0 \\ -i\frac{1}{2}(3g-g_1)\beta H & E+R & 0 & 0 \\ 0 & 0 & E-R & +\frac{1}{2}i(3g-g_1)\beta H \\ 0 & 0 & -\frac{1}{2}i(3g-g_1)\beta H & E-R \end{bmatrix} \end{array}, \tag{2.17}$$

where R is defined by $H_{13}=Re^{i\varphi}$. This is clearly diagonal when $H=0$, and as shown by the reduced form of $\Gamma_1(RI)$ the states may be labeled by E from the unitary subgroup and by plus or minus according to the sign of φ entering in the transformation properties under RI. Similarly, S_2 must diagonalize $\tilde{\mathcal{H}}(\Gamma_2)$ by group theory and the reason it can is that the information

$$H_{14}=\langle 1|\mathcal{H}|4\rangle=\langle RI1|\mathcal{H}|RI4\rangle^*=H_{32} \tag{2.18}$$

is contained in the antiunitary symmetry operators. Insertion of this into $\tilde{\mathcal{H}}(\Gamma_2)$, remembering that H_{14} and H_{23} have been shown to be real, produces, for $H=0$, two subblocks, each having equal on-diagonal elements, and this form is clearly diagonalized by S_2 if θ_1 and θ_2 are chosen as the phases of R_1 and R_2, respectively. Carrying out the transformation, including magnetic-field terms, and using trigonometric manipulation to put the resulting mag-

netic-interaction matrix elements in the form of a magnitude and a phase, yields

$$S_2^{\dagger}\mathfrak{H}(\Gamma_2)S_2=\begin{array}{c} \begin{matrix} |A_1\rangle & |A_1^+\rangle & |A_2^+\rangle & |A^{2-}\rangle \end{matrix} \\ \begin{bmatrix} E+H_{14}+R_1 & 0 & \frac{1}{2}\tilde{g}\beta H\sin\frac{1}{2}\Delta\varphi e^{ix_1} & \frac{1}{2}\tilde{g}\beta H\cos\frac{1}{2}\Delta\varphi e^{ix_2} \\ 0 & E+H_{14}-R_1 & \frac{1}{2}\tilde{g}\beta\ \tilde{g}\cos\frac{1}{2}\Delta\varphi^{-ix_2} & \frac{1}{2}\tilde{g}\beta H\sin\frac{1}{2}\Delta\varphi^{ix_1} \\ \frac{1}{2}\tilde{g}\beta H\sin\frac{1}{2}\Delta\varphi e^{-ix_1} & \frac{1}{2}\tilde{g}\beta H\cos\frac{1}{2}\Delta\varphi e^{+ix_2} & E-H_{14}+R_2 & 0 \\ \frac{1}{2}\tilde{g}\beta H\cos\frac{1}{2}\Delta\varphi e^{-ix_2} & \frac{1}{2}\tilde{g}\beta\ \tilde{g}\sin\frac{1}{2}\Delta\varphi e^{-ix_1} & 0 & E-H_{14}-R_2 \end{bmatrix} \end{array}, \tag{2.19}$$

with $\tilde{g}\equiv(g_2-3g)$, $\Delta\varphi\equiv\varphi_1-\varphi_2$, $\chi_1\equiv\frac{1}{2}(\pi-\Delta\varphi)$, and $\chi_2\equiv\frac{1}{2}(\varphi_1+\varphi_2)$. For $H=0$, this is diagonal and the states are labeled by A_1 and A_2 from the unitary subgroup and by plus and minus according to the sign with which φ_1 and φ_2 appear in the transformation properties under RI.

Considering the Γ_1 results, it is immediately evident that for $H\neq0$, each E level is split uniformly by an amount $|3g-g_1|\beta H$. The eigenvectors and eigenvalues are, by inspection,

$$2^{-1/2}\{|xE^{\pm}\rangle-i|yE^{\pm}\rangle\}\text{ with energy }(E\pm R)+\tfrac{1}{2}(3g-g_1)\beta H, \tag{2.20}$$

and

$$2^{-1/2}\{|xE^{\pm}\rangle+i|yE^{\pm}\rangle\}\text{ with energy }(E\pm R)-\tfrac{1}{2}(3g-g_1)\beta\,\tilde{g}.$$

The field exactly decouples the single-ion excitations of up-spin sites from those of down-spin sites as can be seen from the $H\neq0$ eigenvectors; for example,

$$2^{-1/2}\{|xE^{+}\rangle-i|yE^{+}\rangle\}=2^{-1/2}[|4\rangle+e^{-i\varphi}|2\rangle]. \tag{2.21}$$

This is expected since only $E_{13}=H_{42}$ is nonzero for the Γ_1 states anyway. The form of the $H\neq0$ eigenvectors also clearly shows that transitions to these levels are circularly polarized. Both g and g_1 are expected to be near 2 and positive, making $3g-g_1$ positive, so that if circularly polarized light is propagated along the direction of positive H, right circularly polarized light which transforms like $x+iy$ will excite the states that lose energy in the presence of H and left circularly polarized light which transforms like $x-iy$ will excite the states that gain energy in the presence of H.

The analysis for the Γ_4 functions is very similar to the one for the Γ_1 functions, since both give rise, at $\mathbf{k}=0$, to two E excitons, and the Γ_4 results can be obtained from the Γ_1 results with the following substitutions.

(1) The linear combinations of $|1\rangle$, $|2\rangle$, $|3\rangle$, and $|4\rangle$ that transformed as x for Γ_1 transform as y for Γ_4, and vice versa.

(2) The magnetic splitting factor $3g-g_1$ for Γ_1 is replaced by $3g+g_1$ for Γ_4.

Thus the splitting factors for the Γ_4E levels are expected to be significantly larger than those for the Γ_1E levels, and the circular polarization properties of transitions to the two kinds of E levels should be reversed. The reversal of polarizations is not very surprising since the Γ_1 and Γ_4 levels arise from excited states of opposite spin relative to the ground-state spin. In fact, the splitting factor sign and magnitude differences are apparent from an inspection of Fig. 5, keeping in mind that only H_{13} and H_{24} are nonzero. Lines 1 and 4 have the linear polarizations predicted for transitions to E levels and both have the same splitting factor, suggesting that they are both either Γ_1 or Γ_4 levels, rather than being one of each as in van der Ziel's assignment. Foner's antiferromagnetic resonance work[16] has shown that $g=1.99$, and since $g_1=g_4$ is expected to be about 2 the fact that the observed splitting factor of 4.6 is less than $3\times1.99=5.97$ indicates that lines 1 and 4 are transitions to Γ_1E levels. With this assignment g_1 is measured to be $5.97-4.6=1.37$. The departure of g_1 from the spin-only value 2 is in the opposite direction than occurs for the same single-ion level of Cr^{3+} in Al_2O_3 (ruby). This is reasonable since it may be noted from Foner's determination[16] of the single-ion anisotropy that the trigonal crystal field parameter v' that enters strongly and linearly in determining g_1 is of opposite sign to that in ruby. The result of an experiment, which will be described in Sec. IV, determining the circular polarization of lines 1 and 4 in an axial spectrum is that both lines are polarized the same, and that the polarizations are those predicted for Γ_1 levels. In view of this experimental evidence there seems little doubt that the reassignment of lines 1 and 4 as transitions to Γ_1E levels is correct, and, as previously stated in Sec. I, this change eliminates several other difficulties present in van der Ziel's assignments. Then the energy separation of lines 1 and 4 is the Γ_1 Davydov splitting $2|H_{13}|$; since the observed separation is 183 cm^{-1}, $|H_{13}|$ is measured to be 91.5 cm^{-1}. The origin of this sizeable interaction will be discussed in Sec. III.

Considering now the results for Γ_2, it can be noted that they differ significantly from those for Γ_3 only in that $\tilde{g}$ is replaced by $-(3g+g_3)$ in the magnetic-interaction matrix elements. Transitions to both the A_2^+ and A_2^- Γ_2 states are expected, and it is consistent with the observed linear polarizations of lines 3 and 2 to assign them as these transitions. As pointed out by van der Ziel, the behavior of line 2′ suggests it is a transition to an A_1 state being coupled by the applied magnetic field to a nearby A_2 state and thus becoming observable. Inspection of the $H=0$ Γ_2 states' energies

[16] S. Foner, Phys. Rev. 130, 183 (1963).

uggests that the two states involved are A_1^- and A_2^-. Evidently the Hamiltonian for $H\neq 0$ cannot be diagonalized algebraically, but in the approximation that the A_1^- and A_2^- states couple strongly only to each other, a 2×2 matrix results and the difference of the eigenvalues $\Delta\lambda$ is easily found to be

$$(\Delta\lambda)^2=(R_1-R_2-2H_{14})^2+(\tilde{g}\beta\sin\tfrac{1}{2}\Delta\varphi)^2H^2. \quad (2.22a)$$

van der Ziel has found empirically that the separation of lines 2 and 2′ obeys the relation

$$(\Delta\lambda \text{ in cm}^{-1})^2 = (3.75)^2+(1.435)^2[H/(10\text{ kG})]^2, \quad (2.22b)$$

indicating that the approximate diagonalization above is valid. Comparing the two relations shows, setting $\beta=0.46\text{ cm}^{-1}/(10\text{ kg})$,

$$|(3g-g_2)\sin\tfrac{1}{2}\Delta\varphi| = 1.435/0.46 = 3.12, \quad (2.23)$$

and if $\sin\frac{1}{2}\Delta\varphi$ is ± 1 ($\Delta\varphi=\pm 180°$), then g_2 is $3\times 1.99-3.12=2.85$. It may be recalled that g_1 was determined from the splitting of the $\Gamma_1 E$ levels to be 1.37, which is less than 2.0 by 0.63. This amount of asymmetry about 2 of g_1 and g_2 is very reasonable and there is no *a priori* reason not to set $\Delta\varphi=\pm 180°$. If this is done the approximate $A_1^--A_2^-$ diagonalization above becomes exact since the other couplings of these states (to A_2^+ and A_1^+, respectively) are proportional to $\cos\frac{1}{2}\Delta\varphi=\cos\pm 90°=0$. In any event, these other couplings are certainly ineffectual because the $H=0$ separation of the levels involved is large compared to $\tilde{g}\beta H\cos\frac{1}{2}\Delta\varphi$. It may also be noted that the size of the coupling factor favors the interpretation that Γ_3 states are not involved since then $3g+g_2$ would enter instead of $3g-g_2$. Since line 3, assigned as a transition to the A_2^+ state, is unaffected within the experimental error of 0.5 cm^{-1} even by an applied field of 50 kG, then it must be that the unobserved A_1^+ state to which it couples when $H\neq 0$ is at least, using second-order perturbation theory,

$$\frac{[\frac{1}{2}\tilde{g}\beta(H=50\text{ kG})\sin\frac{1}{2}\Delta\varphi]^2}{0.5\text{ cm}^{-1}}=\tfrac{1}{2}(0.46\times 5\times 3.12)^2 = 26\text{ cm}^{-1} \quad (2.24)$$

away from the A_2^+ level. Then there are two Γ_2 Davydov splitting patterns consistent with experiment; they are shown in Fig. 6, labeled case 1 and case 2. Under the assumptions that the $A_2^+-A_1^+$ separation is 30 cm^{-1} and that $\Delta\varphi=\pm 180°$, the values of H_{12}, H_{13}, and H_{14} for the two cases are given in Table I. The two cases are distinguished by the sign of H_{14}, the relative sign between H_{12} and H_{13}, or the size of H_{13}. It is worth noting that it is possible to fit the spectrum by reversing the values of H_{13} and H_{12} in each case, but this makes $\Delta\varphi=0$, which causes the wrong levels to be coupled by the field. Thus the magnetic field behavior forces an interpretation with $\Delta\varphi\simeq 180°$, implying $|H_{13}|>|H_{12}|$. As will be seen in Sec. III, this result is consistent with a microscopic analysis of the interactions. The last entry in Table I, Δ_{si}, is the deduced energy separation of the two single-ion levels being Davydov-split, assuming the A and E excitons have small or nearly equal dispersion. This separation is due to the combined effects of exchange and trigonal field plus spin-orbit splitting, and is perhaps significant because McClure's measurement of the $^4T_2$ band splitting gives the trigonal field parameter v as about -700 cm^{-1}. This implies,[17] assuming both levels have equal exchange splittings, that Δ_{si} is $+15$–20 cm^{-1}. As will be seen in Sec. III, the exchange splittings of the two single-ion levels are, in fact, expected to be nearly equal so the sign of the splitting would seem to favor case 2. It is to be emphasized that the values in Table I are given merely to provide an indication of the sizes of the couplings and cannot be taken as firm experimental values because the location of the A_1^+ level is not known.

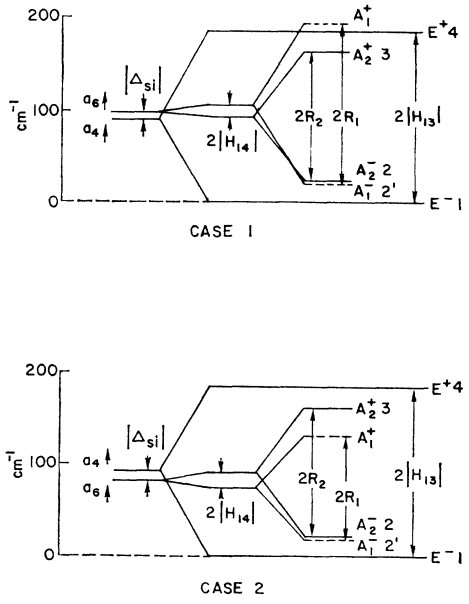

FIG. 6. Two possible Davydov splitting patterns consistent with both theory and experiment. Sign of Δ_{si} favors case 2.

TABLE I. Assignment of experimental values of parameters for two cases shown in Fig. 6.

Case 1	Case 2
$H_{14}=+$ 6.5 cm^{-1}	$H_{14}=-$ 8.5 cm^{-1}
$H_{13}=\pm$78.5 cm^{-1}	$H_{13}=\pm$63.5 cm^{-1}
$H_{12}=\pm$ 8.5 cm^{-1}	$H_{12}=\mp$ 6.5 cm^{-1}
$\Delta\varphi=\mp 180°$	$\Delta\varphi=\mp 180°$
$\Delta_{si}=-$ 7.5 cm^{-1}	$\Delta_{si}=+$ 7.5 cm^{-1}

[17] R. M. Macfarlane, J. Chem. Phys. 47, 2066 (1967).

III. INTERION INTERACTIONS

In contrast to the discussion of Sec. II, which emphasized the role of crystal symmetry in determining the optical absorption spectrum, it is the purpose of this section to investigate the interactions responsible for determining the spectrum with the twofold purpose of determining if the new assignments involve quantitatively sensible energy separations and gaining information from the observed spectrum. In particular, three quantities will be investigated, the single-ion exchange splittings, the matrix elements involved in van der Ziel's proposed mechanism for the intensities of lines 3 and 4 in his assignments, and the transfer-of-excitation matrix elements pertinent to the assignments proposed in this paper.

Interactions between electrons on different ions are of two principal kinds, the spin-independent electrostatic interaction of charge with charge, and the spin-dependent exchange interactions associated with the requirement of using antisymmetrized crystal states. The essential point to be made in the present discussion is that fundamentally the interactions occur not between pairs of ions but between various pairs of electrons bound into the ion states and this configuration interaction aspect of the problem cannot be ignored. Thus the first-principles interaction Hamiltonian for ions at $\mathbf{R}$ and $\mathbf{R}'$ has the form

$$\begin{aligned}&\mathcal{H}(\mathbf{R},\mathbf{R}')\\&=\sum_{n_1,n_2,n_3,n_4}\sum_{\sigma,\sigma'}[K(\mathbf{R},\mathbf{R}';n_1n_2n_3n_4)\\&\quad\times a^\dagger(\mathbf{R}\sigma n_1)a^\dagger(\mathbf{R}'\sigma' n_2)a(\mathbf{R}'\sigma' n_3)a(\mathbf{R}\sigma n_4)\\&\quad+J(\mathbf{R},\mathbf{R}';n_1n_2n_3n_4)\\&\quad\times a^\dagger(\mathbf{R}\sigma n_1)a^\dagger(\mathbf{R}'\sigma' n_2)a(\mathbf{R}'\sigma n_3)a(\mathbf{R}\sigma' n_4)],\end{aligned}\tag{3.1}$$

where $a^\dagger$ and a are single-electron (fermion) creation and annihilation operators for Wannier functions or orthogonalized (from site to site) covalent crystal-field functions labeled by ion site $\mathbf{R}$, spin σ, and orbital index n, which runs over the single-electron functions needed to describe the magnetic shell electrons. By inspecting the spin indices on the operators in $\mathcal{H}(\mathbf{R},\mathbf{R}')$ it is evident that the first term represents the spin-independent electrostatic interaction of two electrons on different ions, and the second term represents a spin-dependent interaction of two electrons on different ions. The coefficients K and J may be related to more fundamental parameters by making a specific model of the interactions, for example, Anderson's superexchange theory,[18] for which it can be shown that

$$\begin{aligned}K(\mathbf{R},\mathbf{R}';klmn)&\equiv\tfrac{1}{2}\langle k\mathbf{R},l\mathbf{R}'|\frac{e^2}{|\mathbf{r}-\mathbf{r}'|}|n\mathbf{R},m\mathbf{R}'\rangle\\&=\int\int d\mathbf{r}d\mathbf{r}'\varphi_k^*(\mathbf{r}-\mathbf{R})\varphi_l^*(\mathbf{r}'-\mathbf{R}')\frac{e^2}{|\mathbf{r}-\mathbf{r}'|}\\&\quad\times\varphi_n(\mathbf{r}-\mathbf{R})\varphi_m(\mathbf{r}'-\mathbf{R}')\end{aligned}\tag{3.2}$$

and

$$\begin{aligned}J(\mathbf{R},\mathbf{R}';klmn)&=b(l\mathbf{R}',n\mathbf{R})b(k\mathbf{R},m\mathbf{R}')/U\\&\quad-\tfrac{1}{2}\langle k\mathbf{R},l\mathbf{R}'|\frac{e^2}{|\mathbf{r}-\mathbf{r}'|}|m\mathbf{R}',n\mathbf{R}\rangle,\end{aligned}\tag{3.3}$$

where $b(n\mathbf{R},n'\mathbf{R}')=\langle n\mathbf{R}|\mathcal{H}_B|n'\mathbf{R}'\rangle$ is the one-electron transfer matrix element of the band Hamiltonian $\mathcal{H}_B$ from whose eigenfunctions the Wannier states are constructed, and U is the cost in energy to remove an electron from the state $n'\mathbf{R}'$ and place it in the state $n\mathbf{R}$. The b terms give rise to antiferromagnetic kinetic exchange while the Coulomb exchange term in J is ferromagnetic. It should be mentioned that in the Anderson theory, a third term involving b^2/U appears in $\mathcal{H}(\mathbf{R},\mathbf{R}')$, but since this term does not affect the quantities of interest in this discussion it was omitted. Since the results to be obtained in this section do not depend on the detailed nature of K and J, this aspect will not be pursued further.

The information that the interacting electrons have already been bound by strong intra-ion forces into ion states is inserted in the problem by computing matrix elements of the full interaction Hamiltonian

$$\mathcal{H}_I=\sum_{\mathbf{R}\neq\mathbf{R}'}\mathcal{H}(\mathbf{R},\mathbf{R}')\tag{3.4}$$

between the crystal states defined in Sec. II. Because $\mathcal{H}_I$ involves only pairwise ion interactions, these matrix elements are of only three types: those that are diagonal, those between crystal states where the state of one ion is changed, and those between crystal states where the state of two ions is changed. Explicit expressions for these three kinds of matrix elements are, respectively,

$$\begin{aligned}&\langle\mu\mathbf{R}_{01},\cdots,\mu\mathbf{R}_{Np}|\mathcal{H}_I|\mu\mathbf{R}_{01},\cdots,\mu\mathbf{R}_{Np}\rangle\\&=\sum_{\mathbf{R}_{ni}\neq\mathbf{R}_{mj}}\langle\mu\mathbf{R}_{ni},\mu\mathbf{R}_{mj}|\mathcal{H}(\mathbf{R}_{ni},\mathbf{R}_{mj})\\&\qquad+\mathcal{H}(\mathbf{R}_{mj},\mathbf{R}_{ni})|\mu\mathbf{R}_{ni},\mu\mathbf{R}_{mj}\rangle,\end{aligned}\tag{3.5}$$

$$\begin{aligned}&\langle\mu\mathbf{R}_{01},\cdots,\mu\mathbf{R}_{ni},\cdots,\mu\mathbf{R}_{Np}|\mathcal{H}_I\\&\qquad\times|\mu\mathbf{R}_{01},\cdots,\mu'\mathbf{R}_{ni},\cdots,\mu\mathbf{R}_{Np}\rangle\\&=\sum_{\mathbf{R}_{mj}}\langle\mu\mathbf{R}_{mj},\mu\mathbf{R}_{ni}|\mathcal{H}(\mathbf{R}_{mj},\mathbf{R}_{ni})\\&\qquad+\mathcal{H}(\mathbf{R}_{ni},\mathbf{R}_{mj})|\mu\mathbf{R}_{mj},\mu\mathbf{R}_{ni}\rangle,\end{aligned}\tag{3.6}$$

and

$$\begin{aligned}&\langle\mu\mathbf{R}_{01},\cdots,\mu\mathbf{R}_{ni},\cdots,\mu\mathbf{R}_{mj},\cdots,\mu\mathbf{R}_{Np}|\mathcal{H}_I\\&\qquad\times|\mu\mathbf{R}_{01},\cdots,\mu'\mathbf{R}_{ni},\cdots,\mu'\mathbf{R}_{mj},\cdots,\mu\mathbf{R}_{Np}\rangle\\&=\langle\mu\mathbf{R}_{mj},\mu\mathbf{R}_{ni}|\mathcal{H}(\mathbf{R}_{mj},\mathbf{R}_{ni})\\&\qquad+\mathcal{H}(\mathbf{R}_{ni},\mathbf{R}_{mj})|\mu'\mathbf{R}_{mj},\mu'\mathbf{R}_{ni}\rangle.\end{aligned}\tag{3.7}$$

[18] P. W. Anderson, Phys. Rev. **115**, 2 (1959).

From the form of $\mathcal{H}(\mathbf{R},\mathbf{R}')$, it is easy to show, by anticommuting the operators and relabeling dummy sum indices, that $\mathcal{H}(\mathbf{R},\mathbf{R}')=\mathcal{H}(\mathbf{R}'\mathbf{R})$, so that in the matrix elements above only $2\mathcal{H}(\mathbf{R}_{ni},\mathbf{R}_{mj})$ need be used. The factors of $\frac{1}{2}$ needed to avoid double counting are to be placed in the coefficients K and J.

To compute a matrix element the appropriate two-ion states must be constructed as antisymmetrized products of the linear combinations of Slater determinants that diagonalize the single-ion Hamiltonian $\mathcal{H}(\mathbf{R}_{ni})$. The form of a single-ion eigenstate is

$$|\mu\mathbf{R}_{mj}\rangle=\sum_{n1,\sigma1}\cdots\sum_{nl,\sigma l}A(\mu\mathbf{R}_{mj};n_1\sigma_1,\cdots,n_l\sigma_l)\times a^\dagger(\mathbf{R}_{mj}\sigma_1 n_1)\cdots a^\dagger(\mathbf{R}_{mj}\sigma_l n_l)|0\rangle, \quad (3.8)$$

where l is the number of electrons on the ion, and the coefficients A are determined in the course of the single-ion crystal-field calculation. The form of a two-ion state is then

$$|\mu\mathbf{R}_{mj},\mu\mathbf{R}_{ni}\rangle=\sum_{k1,\epsilon1}\cdots\sum_{kl,\epsilon l}\sum_{n1,\sigma1}\cdots\sum_{nl,\sigma l}A(\mu\mathbf{R}_{mj};k_1\epsilon_1,\cdots,k_l\epsilon_l)\times A(\mu\mathbf{R}_{ni};n_1\sigma_1,\cdots,n_l\sigma_l)a^\dagger(\mathbf{R}_{mj}\epsilon_1 k_1)\cdots a^\dagger(\mathbf{R}_{mj}\epsilon_l k_l)\times a^\dagger(\mathbf{R}_{ni}\sigma_1 n_1)\cdots a^\dagger(\mathbf{R}_{ni}\sigma_l n_l)|0\rangle, \quad (3.9)$$

which is a linear combination of $2l$-electron Slater determinants for the electrons of the two ions, the coefficient of each such determinant being a product of the coefficients of the single-ion l-electron determinants of which it is built. Using Eqs. (3.1) and (3.9), two-ion matrix elements have the form

$$\begin{aligned}\langle\mu\mathbf{R}_{mj},\mu\mathbf{R}_{ni}|\,2\mathcal{H}(\mathbf{R}_{ni},\mathbf{R}_{mj})\,|\mu'\mathbf{R}_{mj},\mu'\mathbf{R}_{ni}\rangle&=\sum_{n1,n2,n3,n4}\sum_{\sigma,\sigma'}\sum_{m1,\sigma1}\cdots\sum_{ml,\sigma l}\sum_{m1',\sigma1'}\cdots\sum_{ml',\sigma l'}\sum_{k1,\epsilon1}\cdots\sum_{kl,\epsilon l}\sum_{k1',\epsilon1'}\cdots\sum_{kl',\epsilon l'}A^*(\mu\mathbf{R}_{mj};k_1\epsilon_1,\cdots,k_l\epsilon_l)\\&\times A^*(\mu\mathbf{R}_{ni};m_1\sigma_1,\cdots,m_l\sigma_l)A(\mu'\mathbf{R}_{mj};k_1'\epsilon_1',\cdots,k_l'\epsilon_l')A(\mu'\mathbf{R}_{ni};m_1'\sigma_1',\cdots,m_l'\sigma_l')\\&\times\langle0|\,a(\mathbf{R}_{ni}\sigma_l m_l)\cdots a(\mathbf{R}_{ni}\sigma_1 m_1)a(\mathbf{R}_{mj}\epsilon_l k_l)\cdots a(\mathbf{R}_{mj}\epsilon_1 k_1)\\&\times[2K(\mathbf{R}_{mj},\mathbf{R}_{ni};n_1n_2n_3n_4)a^\dagger(\mathbf{R}_{mj}\sigma n_1)a^\dagger(\mathbf{R}_{ni}\sigma' n_2)a(\mathbf{R}_{ni}\sigma' n_3)a(\mathbf{R}_{mj}\sigma n_4)\\&+2J(\mathbf{R}_{mj},\mathbf{R}_{ni};n_1n_2n_3n_4)a^\dagger(\mathbf{R}_{mj}\sigma n_1)a^\dagger(\mathbf{R}_{ni}\sigma' n_2)a(\mathbf{R}_{ni}\sigma n_3)a(\mathbf{R}_{mj}\sigma' n_4)]\\&\times a^\dagger(\mathbf{R}_{mj}\epsilon_1'k_1')\cdots a^\dagger(\mathbf{R}_{mj}\epsilon_l'k_l')a^\dagger(\mathbf{R}_{ni}\sigma_1'm_1')\cdots a^\dagger(\mathbf{R}_{ni}\sigma_l'm_l')|0\rangle. \quad (3.10)\end{aligned}$$

The matrix element of creation and annihilation operators is computed in the usual way, either by anticommuting all annihilation operators to the right or all creation operators to the left. The result is a linear combination of K's and J's. At this point it is convenient to observe that there are two simple selection rules on this matrix element. First, because the interactions involve electrons by twos, one on each ion, the two $2l$-electron Slater determinants being connected can differ at most by the change of state of one electron on each ion. Secondly, inspection of the indices on the operators in Eq. (3.1) shows that for the direct term (K) the spin of the state on an ion cannot be changed, but there is no constraint between the spins on the two ions, while for the exchange term (J) the spin on an ion can change so long as the initial-state spin on one ion is the same as the final-state spin on the other ion. These rules can be used to eliminate many matrix elements by inspection, as will be seen later.

Cr_2O_3, with the Cr^{3+} ion, is a nice example for the general approach just described, because the single-ion problem has been treated in elaborate detail by many workers due to the great interest in the Cr^{3+} ion in ruby. Further, it so happens that the single-ion states giving rise to the excitons discussed in Sec. II have a very simple structure. In the cubic approximation where trigonal crystal field and spin-orbit effects are neglected, the ground- and excited-state manifolds are, respectively, $^4A_2$ and ^2E. Inspection of numerical eigenvectors of the Cr^{3+} Al_2O_3 Hamiltonian in the Sugano-Peter[19] approximation shows that other cubic states are mixed into $^4A_2$ and ^2E by the trigonal field and spin-orbit coupling with coefficients that are always less than 10^{-1}. This is also true of the amount of mixing of $^4A_2$ and ^2E into each other. The order of magnitude of these results is not expected to change much for the Cr^{3+} ion in Cr_2O_3 as the optical spectrum suggests that the crystal-field parameters in ruby and Cr_2O_3 are of comparable magnitudes. Thus, to a very good approximation the single-ion states entering the present discussion may be taken as cubic $^4A_2$ and ^2E functions, chosen to transform irreducibly according to C_3 double group representations so that no off-diagonal crystal-field matrix elements will exist within a manifold. These functions are linear combinations of Slater determinants in which each of the three t_{2g} cubic $3d$ orbitals, commonly labeled ξ, η, and ζ, are singly oc-

[19] S. Sugano and M. Peter, Phys. Rev. 122, 318 (1961).

cupied. The linear combinations are easily found[20] to be

$$
\begin{aligned}
&|{}^4A_2+\tfrac{3}{2},a_6\uparrow\rangle=|\uparrow\uparrow\uparrow\rangle,\\
&|{}^4A_2+\tfrac{1}{2},a_5\uparrow\rangle=3^{-1/2}[|\uparrow\uparrow\downarrow\rangle+|\uparrow\downarrow\uparrow\rangle+|\downarrow\uparrow\uparrow\rangle],\\
&|{}^4A_2-\tfrac{1}{2},a_4\downarrow\rangle=3^{-1/2}[|\downarrow\uparrow\uparrow\rangle+|\uparrow\downarrow\uparrow\rangle+|\downarrow\downarrow\uparrow\rangle],\\
&|{}^4A_2-\tfrac{3}{2},a_6\downarrow\rangle=|\downarrow\downarrow\downarrow\rangle,\qquad(3.11)\\
&|{}^2E+\tfrac{1}{2}u_+,a_6\uparrow\rangle=3^{-1/2}[e^{i5\pi/6}|\uparrow\downarrow\uparrow\rangle+e^{i\pi/6}|\downarrow\uparrow\uparrow\rangle\\
&\qquad\qquad+e^{i3\pi/2}|\uparrow\uparrow\downarrow\rangle],\\
&|{}^2E-\tfrac{1}{2}u_-,a_6\downarrow\rangle=3^{-1/2}[e^{i\pi/6}|\downarrow\uparrow\downarrow\rangle+e^{i5\pi/6}|\uparrow\downarrow\downarrow\rangle\\
&\qquad\qquad+e^{i3\pi/2}|\downarrow\downarrow\uparrow\rangle],\\
&|{}^2E-\tfrac{1}{2}u_+,a_5\downarrow\rangle=3^{-1/2}[e^{i5\pi/6}|\downarrow\uparrow\downarrow\rangle+e^{i\pi/6}|\uparrow\downarrow\downarrow\rangle\\
&\qquad\qquad+e^{i3\pi/2}|\downarrow\downarrow\uparrow\rangle],\\
&|{}^2E+\tfrac{1}{2}u_-,a_4\uparrow\rangle=3^{-1/2}[e^{i\pi/6}|\uparrow\downarrow\uparrow\rangle+e^{i5\pi/6}|\downarrow\uparrow\uparrow\rangle\\
&\qquad\qquad+e^{i3\pi/2}|\uparrow\uparrow\downarrow\rangle],
\end{aligned}
$$

where

$$|\sigma_1,\sigma_2,\sigma_3\rangle\equiv a^\dagger(\sigma_1\xi)a^\dagger(\sigma_2\eta)a^\dagger(\sigma_3\zeta)|0\rangle.$$

The labeling on the ion functions gives the cubic origin, the trigonal representation, and an arrow to indicate the sign of the z component of spin. Because the departure of the true eigenstates from those above is so small, all large interion effects should be found using these states.

Following the discussion of Sec. II, five single-ion exchange splittings of the ${}^4A_2$ and ${}^2E$ levels can be defined as

$$
\begin{aligned}
&|{}^4A_2a_4\downarrow\mathbf{R}_{mj}|-|{}^4A_2a_6\downarrow\mathbf{R}_{mj}|,\\
&|{}^4A_2a_5\uparrow\mathbf{R}_{mj}|-|{}^4A_2a_4\downarrow\mathbf{R}_{mj}|,\\
&|{}^4A_2a_6\uparrow\mathbf{R}_{mj}|-|{}^4A_2a_5\uparrow\mathbf{R}_{mj}|,\qquad(3.12)\\
&|{}^2Ea_4\uparrow\mathbf{R}_{mj}|-|{}^2Ea_5\downarrow\mathbf{R}_{mj}|,\\
&|{}^2Ea_6\uparrow\mathbf{R}_{mj}|-|{}^2Ea_6\downarrow\mathbf{R}_{mj}|,
\end{aligned}
$$

where $|\mu\mathbf{R}_{mj}|\equiv\langle\mu\mathbf{R}_{mj}|\mathcal{H}_I|\mu\mathbf{R}_{mj}\rangle$ and $\mathbf{R}_{mj}$ is taken as a down-spin site. As in Sec. II, $|\mu\mathbf{R}_{mj}\rangle$ here denotes a crystal state that differs from $|G\rangle$ only by the excitation of the ion at $\mathbf{R}_{mj}$ from its state in $|G\rangle$ to the state μ. The matrix elements required are of the type of Eq. (3.5) and hence are sums of two-ion diagonal matrix elements. Since all other terms are the same for all $|\mu\mathbf{R}_{mj}|$ and disappear in taking differences, only the terms involving $\mathbf{R}_{mj}$ need be computed, and these are of two kinds, depending on whether the ion other than $\mathbf{R}_{mj}$ is an up- or down-spin site. Using Eqs. (3.10)–(3.12), and (3.5), the contribution to all five exchange splittings of Eq. (3.12) from up- and down-spin neighbors is computed to be $\delta(\mathbf{R},\mathbf{R}')$ and $-\delta(\mathbf{R},\mathbf{R}')$, respectively, where $\delta(\mathbf{R},\mathbf{R}')$ is given by

$$\delta(\mathbf{R},\mathbf{R}')\equiv\tfrac{2}{3}\sum_{i,j=\xi,\eta,\zeta}J(\mathbf{R},\mathbf{R}';ijji),\qquad(3.13)$$

which is an eminently sensible result. Since it is true that the interactions with arbitrary up- and down-spin neighbors cause equal ground and excited-state exchange splittings, then the actual splittings obtained by summing the contributions from all ions will also be the same for the ground and excited states. This result would be changed if the effects of admixtures of other cubic crystal-field states into the ${}^4A_2$ and ${}^2E$ states were included. These contributions, for the case of the ground-state energy, are precisely the ones Good-enough and Stickler[21] recently introduced *ad hoc* and referred to as excitonic superexchange terms, and they appear rather naturally in this formulation of interion interactions. The reason for the term "excitonic super-exchange" is that admixtures of higher-lying cubic states into the ground state would lead to two-ion contributions to $\langle G|\mathcal{H}_I|G\rangle$ of the form

$$A^2\langle\Gamma\mathbf{R},{}^4A_2\mathbf{R}'|\mathcal{H}(\mathbf{R},\mathbf{R}')|{}^4A_2\mathbf{R},\Gamma\mathbf{R}'\rangle,\qquad(3.14)$$

where Γ is the admixed state and A is the admixture coefficient, and this is the sort of matrix element to be considered below in discussing transfer-of-excitation in the exciton problem. Contributions of this sort to the exchange splittings in Cr_2O_3 discussed here are not expected to be large because the admixture coefficients are so small. It is unfortunate that the excitons associated with the upper excited levels are not observable in Cr_2O_3, as discussed in Sec. II, since the result of equal ground- and excited-state exchange splittings cannot then be checked experimentally. However, the expression for δ will be useful later in discussing the size of certain transfer-of-excitation matrix elements.

In order to explain the observed large intensities of lines 3 and 4 in his assignments, van der Ziel has proposed that the interion interactions may cause an effective single-ion coupling of the upper states for which a single-ion intensity mechanism does not exist and the lower excited states, for which a single-ion intensity mechanism does exist. A generalization that includes this possibility is to ask if there are matrix elements between upper excited-state excitons and lower excited-state excitons of the same symmetry, for example, between Γ_4E excitons and Γ_1E excitons. This would involve matrix elements between sublattice excitons generated from upper and lower excited states, which, from Eq. (2.7) would have the form

$$
\begin{aligned}
&\langle\Gamma\mathbf{k}i|\mathcal{H}|\Gamma'\mathbf{k}'j\rangle\\
&\qquad=\delta_{\mathbf{k}\mathbf{k}'}\sum_{\mathbf{T}_{mn}}e^{-i\mathbf{k}\cdot\mathbf{T}_{mn}}\langle\mathbf{R}_{ni}\Gamma|\mathcal{H}|\mathbf{R}_{mj}\Gamma'\rangle,\qquad(3.15)
\end{aligned}
$$

where Γ and Γ' are the upper and lower excited states, respectively. Such possibilities can be eliminated using the two selection rules mentioned above. The specific mechanism suggested by van der Ziel is given by the $\mathbf{T}_{mn}=0$ term in Eq. (3.15) for $i=j$, which is a matrix element between crystal states of the type in Eq. (3.6)

[20] J. S. Griffith, *The Theory of Transitional Metal Ions* (Cambridge University Press, London, 1961).

[21] J. B. Goodenough and J. J. Stickler, Phys. Rev. **164**, 768 (1967).

where the two states differ only by the change of the state of one ion. From Eq. (3.11) it is evident that to couple the upper and lower excited states of any ion requires a single-electron spin flip on the ion which can only be done by the exchange term in $\mathcal{H}(\mathbf{R},\mathbf{R}')$, and then only if the initial-state spin on one ion is the same as the final-state spin on the other ion, and vice versa. But since the state of one ion remains the same, its initial and final spins are the same, which forbids a spin flip on the other ion. The other terms in Eq. (3.15) are matrix elements of the type in Eq. (3.7) where the states of two ions change, and describe nonresonant transfer of excitation in which, for example, a down-spin excited state deexcites while an up-spin excited state excites. This always necessitates changing the state of one of the ions from the ground state to an upper excited state, and Eq. (3.11) shows that a forbidden two-electron change on the ion is required. These selection-rule restrictions can be avoided by allowing admixtures of other cubic crystal-field states into ^2E or $^4A_2$, but the size of such contributions is reduced at least by one, and sometimes a product of admixture coefficients A. The intensity obtained from these mechanisms will be nominally proportional to $(AM/\Delta E)^2$, where M is the interion matrix element and ΔE is the single-ion exchange splitting. Even assuming the interion matrix element could be as large as the single-ion exchange splitting, the intensity coefficient would be no more than A^2 or 10^{-2} for the largest A, and this is clearly not adequate to account for the equal order-of-magnitude intensities of lines 3 and 4 compared to lines 1 and 2.

The restriction to single-electron changes on an ion restricts large transfer-of-excitation matrix elements to ones involving the two lower excited states, which differ from the ground state by only a single-electron change. Since this change always involves a single-electron spin flip, only the exchange term is effective, and the spin restrictions on this term allow a nonzero matrix element only for transfer of excitation between ion types 1 and 3 or 2 and 4, where the ground states are the same. These are, it will be recalled from Sec. II, precisely the matrix elements which are measured to be large in the assignments proposed in this paper. The matrix element H_{13}, from Eq. (2.7), is given by

$$H_{13}=\langle \mathbf{k}=0,1\,|\,\mathcal{H}\,|\,\mathbf{k}=0,3\rangle = \sum_{\mathbf{T}_{mn}} \langle \mathbf{R}_{01}\,|\,\mathcal{H}\,|\,\mathbf{T}_{mn}+\boldsymbol{\tau}_{13}\rangle, \qquad (3.16)$$

which is a sum of matrix elements of the type of Eq. (3.7) for transfer of excitation between any particular type-1 ion and all other type-3 ions. The largest transfer-of-excitation matrix elements are expected to occur between the type-1 and type-3 ions that are closest to each other. In Cr_2O_3, a type-1 ion has as its nearest type-3 neighbors six equidistant ions which are its fourth nearest neighbors. These are located three in a plane above the ion and three in a parallel plane below the ion, and the three ions in each plane form equilateral triangles whose centers have the central type-1 ion's c axis passing through them perpendicular to the planes. This situation is illustrated in Fig. 7 by a view parallel to the type-1 ion's c axis, including the six oxygen ions through which coupling to the six neighboring Cr^{3+} ions takes place. The ξ, η, ζ orbitals on each ion are shown schematically and labeled in a fashion consistent with the transformation properties assumed for the single-ion states in Sec. II. The next task will be to evaluate the form of the transfer-of-excitation matrix element between arbitrary ions of types 1 and 3, and when this is done it will be clear that the matrix element is the same for all six nearest type-3 neighbors, so that

$$H_{13}=6H_{13}\text{ (fourth nearest neighbors)} +\text{(farther neighbor terms)}. \qquad (3.17)$$

The pertinent two-ion matrix elements for transfer of excitation between ion types 1 and 3 for the states giving rise to A-like and E-like excitons are, respectively,

$$\langle {}^4A_2a_6\uparrow\mathbf{R}_{m1},{}^2Ea_6\uparrow\mathbf{R}_{n3}\,|\,\mathcal{H}\,|\,{}^2Ea_6\uparrow\mathbf{R}_{m1},{}^4A_2a_6\uparrow\mathbf{R}_{n3}\rangle$$

and (3.18)

$$\langle {}^4A_2a_6\uparrow\mathbf{R}_{m1},{}^2Ea_4\uparrow\mathbf{R}_{n3}\,|\,\mathcal{H}\,|\,{}^2Ea_4\uparrow\mathbf{R}_{m1},{}^4A_2a_6\uparrow\mathbf{R}_{n3}\rangle.$$

Using Eqs. (3.11) and (3.10), these two matrix elements

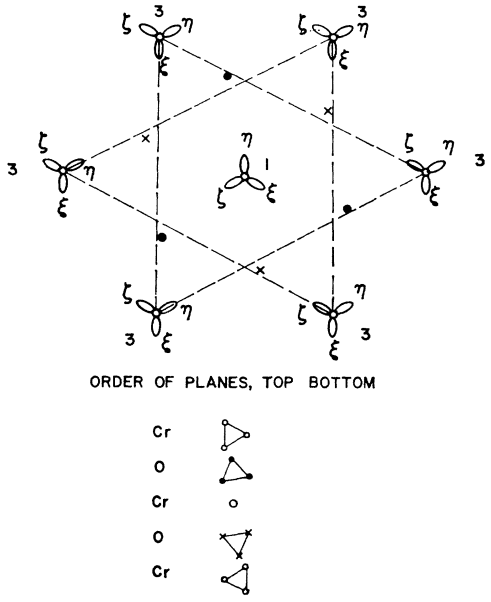

FIG. 7. Schematic diagram, looking parallel to c axis, of cubic orbitals on a type-1 ion and its six nearest-neighbor type-3 ions. Intervening oxygens are also shown. All orbital lobes point down.

are computed to be

$$\tfrac{2}{3}\{[J(\mathbf{R}_{m1},\mathbf{R}_{n3};\,\xi\xi\xi\xi)+J(\mathbf{R}_{m1},\mathbf{R}_{n3};\,\eta\eta\eta\eta)+J(\mathbf{R}_{m1},\mathbf{R}_{n3};\,\zeta\zeta\zeta\zeta)+e^{\pm i\frac{4}{3}\pi}[J(\mathbf{R}_{m1},\mathbf{R}_{n3};\,\eta\xi\xi\eta)+J(\mathbf{R}_{m1},\mathbf{R}_{n3};\,\zeta\eta\eta\zeta)+J(\mathbf{R}_{m1},\mathbf{R}_{n3};\,\xi\zeta\zeta\xi)]+e^{\mp 2\pi i/3}J(\mathbf{R}_{m1},\mathbf{R}_{n3};\,\zeta\xi\xi\zeta)+J(\mathbf{R}_{m1},\mathbf{R}_{n3};\,\xi\eta\eta\xi)+J(\mathbf{R}_{m1},\mathbf{R}_{n3};\,\eta\zeta\zeta\eta)]\}, \quad (3.19)$$

where the upper and lower signs are for A-like and E-like excitons, respectively. Inspection of Fig. 7 shows that the $J(ijji)$ which are spatially equivalent for the six type-3 ions with respect to the intervening oxygen ion always enter these two matrix elements with the same phase factor, so it is evident that the matrix elements for all six neighbors are equal. Both the A-like and E-like matrix elements differ from δ only by the way the individual $J(ijji)$ are phased before being summed, the phasing being such that if all nine were equal both matrix elements would vanish. But all the J's will not be equal since only those orbitals which overlap appreciably due to covalent mixing via an intervening oxygen will have large J's, which orbitals these are depending on their spatial orientations. It seems reasonable, therefore, to estimate that both matrix elements may be roughly as large as $\frac{2}{3}\delta$. Indeed, they could be larger than δ since the $J(ijji)$ may have varying signs. Now δ can be estimated experimentally from studies of the optical absorption or emission spectrum of heavily doped ruby, which shows lines due to various kinds of near-neighbor coupled Cr^{3+} ion pairs. The spectra of fourth near-neighbor pairs, which are the kind involved in the matrix element H_{13}, have been identified and used to determine[22] that the ground state J of $\mathcal{H}_{\text{pair}}=J\mathbf{S}_1\cdot\mathbf{S}_2$ is about 10 cm^{-1}. Since a little thought shows that J and δ are related by $\delta=\frac{3}{2}J$, then both the two-ion matrix elements above are estimated to be on the order of J, or about 10 cm^{-1}. The total E-exciton Davydov splitting, $2H_{13}$, would then be estimated, using Eq. (3.17), as 120 cm^{-1}, which is of the same order of magnitude as the experimental number. The inclusion of spin-orbit and trigonal field admixture of other cubic single-ion states will, as in the result of equal ground- and excited-state exchange splittings, cause some modifications of the results of the transfer of excitation discussion above. In particular, the requirements of the two selection rules that limited transfer-of-excitation to same-spin ions via exchange can be met for both the exchange and direct terms between any ion types when not forbidden by over-all crystal symmetry. The measured small but nonzero values of H_{12} and H_{14} for the A-like excitons indicate that these other possibilities do indeed occur. Because these mechanisms are small, and because many appear to be of comparable magnitude, it is extremely difficult to be more precise about which enter and how for Cr_2O_3.

[22] L. F. Mollenauer and A. L. Schawlow, Phys. Rev. **168**, 309 (1968).

This result concerning the role of exchange as an important transfer-of-excitation mechanism differs sharply from the conclusions of other authors discussing ruby[23] and Cr_2O_3.[8] These authors assumed that the exchange interaction between two Cr^{3+} ions in different states, say, the $^4A_2$ and ^2E, could be adequately represented by a Heisenberg interaction $J\mathbf{S}_1(^4A_2)\cdot\mathbf{S}_2(^2E)$. This interaction reproduces most of the static, or single-ion exchange splitting effects, but gives none of the dynamic transfer-of-excitation effects because a spin operator will not connect states belonging to different total-spin manifolds, a difficulty that does not arise in the application of total-spin Heisenberg exchange to ground-state interactions where the excitons are spin waves and the single-ion states involved are all in the same total-spin manifold. It is by no means a new idea that exchange should be treated in terms of pairs of electrons, but it is only rather recently that serious efforts have been made in this direction, notably in the present discussion, and also by Elliott and Thorpe[24] in discussing orbital effects in ground-state interactions, by Pryce[25] in discussing the pair spectra of ruby, and by Levy,[26] who has recently developed operator techniques that would eliminate much of the messiness encountered in the computations of this section. It should also be emphasized that the results of this section are particular to Cr_2O_3 in two aspects. The first is that the analysis is reasonably tractable because the ground state is almost exactly a cubic approximation orbital singlet with the excited states also being well approximated by cubic functions involving the same three single-electron orbitals as the ground state, and because there are only three electrons per ion. In materials like MnF_2 and CoF_2, where the states of the magnetic ion involve considerable spin-orbit and lower symmetry crystal-field mixing, the formalism outlined at the beginning of this section remains correct, but becomes much more unwieldy to apply. The second aspect particular to Cr_2O_3 is that there are more than two magnetic ions per unit cell, so that the large transfer of excitation between ions whose spins in $|G\rangle$ are the same appears as a $\mathbf{k}=0$ Davydov splitting rather than contributing to exciton dispersion, which is more difficult to observe experimentally.

To conclude, the main result of this discussion is to show that by treating the interion interactions on a first-principles basis, the large transfer-of-excitation mechanism in Cr_2O_3 can be identified as interion exchange between ions whose ground-state spins are the same, and can be estimated, by relating it to single-ion exchange splittings, to be of an order of magnitude consistent with experiment. Finally, it can be observed from inspecting the single-ion states in Eq. (3.11) that the ground-state H_{13}'s are exactly equal to δ, so that large Davydov splittings are also expected in the magnon

[23] G. F. Imbusch, Phys. Rev. **153**, 326 (1967).
[24] R. J. Elliott and M. F. Thorpe, J. Appl. Phys. **38**, 802 (1968).
[25] M. H. L. Pryce, Bull. Am. Phys. Soc. **13**, 415 (1968).
[26] P. M. Levy, Phys. Rev. Letters **20**, 1366 (1968).

spectrum. A careful experimental study of the entire low-energy absorption spectrum of Cr_2O_3 has not been made, but the results of such a study would serve as a good test of the analysis presented in this section.

IV. EXPERIMENTAL

In this section three new kinds of experimental data on lines 1–5 will be presented and discussed: the temperature dependence of the positions and integrated intensities, the uniaxial stress dependence of the positions, and the circular polarizations in an axial Zeeman experiment. In addition, the behavior of line 5 in a transverse Zeeman experiment has not been reported previously.

Single-crystal samples from several different sources were used in these experiments. Flame-fusion-grown boules were obtained from Dr. R. A. Lefever of the Sandia Corporation, flux-grown flakes from Dr. Della M. Roy of the Pennsylvania State University Materials Research Laboratory, and some crystals grown by vapor transport from R. C. Folweiler of the Lexington Laboratory, Cambridge, Massachusetts. The linewidths were largest in the flame-fusion samples, nearly 8 cm^{-1} for line 1, smallest in the flux-grown samples, about 2 cm^{-1} for line 1, and intermediate in the vapor-transport samples, about 5 cm^{-1} for line 1. In this connection it should be mentioned that four pieces of fine structure on line 1 and two pieces on line 2, previously reported by Wickersheim[3] for his flame-fusion samples, were clearly observed in these flame-fusion samples. The flame-fusion samples also display a weak spectrum similar to lines 1–4 but displaced to lower energies about 200 cm^{-1} with different energy separations. These features are not present in the other two samples and are probably due to defects in the flame-fusion crystals. It is unfortunate that the flux-grown samples grow in thin platelets perpendicular to the c axis and hence can only be used in axial experiments where only lines 1 and 4 are observed. Both axial and c-axis-in-the-plane samples were prepared from the flame-fusion and vapor-transport crystals, and except for linewidths, the axial spectra of all three kinds of crystals were the same, confirming the polarizations of the lines. The 4.2°K locations of lines 1–5, in cm^{-1} referred to vacuum, agree with those given by Wickersheim to within 0.5 cm^{-1} for all samples, and are 4–5 cm^{-1} less than the positions reported by van der Ziel.[8] Because the background absorption is very large in Cr_2O_3, presumably because of charge transfer absorption, it is necessary to use rather thin samples in an optical absorption experiment. With the exception of the already thin flux platelets, crystals used were ground and polished to thicknesses ranging from 25 to 110 μ. To be sure that surface-roughness effects were not entering the data, a flame-fusion sample was etched with a molten mixture of $K_2S_2O_7$ and $KHSO_4$ to relax surface strains, and it was found to give the same data as unetched samples.

The temperature-dependent data were taken photometrically, the detector being an RCA 7265 photomultiplier (S-20 surface). A Jarrel-Ash 1-m Ebert spectrograph operated in eighth order, giving a spectral resolution of about 0.2 cm^{-1}, was used principally, although some of the higher-temperature data were taken using a Spex $\frac{3}{4}$ m Czerny-Turner spectrograph in first order, giving a spectral resolution of 1.5 cm^{-1}. Wavelength calibration was obtained from a neon source shone into the spectrometer during the experiment. The samples were mounted in a Linde LNI-15-D cold finger helium Dewar with the sample holder in good thermal contact with two carbon resistors, one for heating and one for measuring the temperature. Accuracy of the temperature measurement is estimated to be 1°K or better between 4.2 and 77.2°K and2.5°K or better between 77.3 and 273°K, which was considered adequate for the studies described here. Temperature stability in the Dewar was better than ± 0.5°K. In order to determine the integrated intensities, the output of the 7265 photomultiplier was fed to a calibrated Hewlett-Packard 7561A logarithmic converter, which drove a chart recorder. Use of the converter gives a signal of known proportionality to αd, α being the absorption coefficient and d the sample thickness, and makes all multiplicative background effects from the optics, instruments, and material additive. A current source inserted in parallel with the photomultiplier preceding the log converter was used to zero out any additive background signal present at the input of the log converter when the carefully masked sample was covered. This correction was small and frequency-independent. The area under the absorption, as recorded by the chart recorder, is then of known proportionality to

$$\int \alpha(\lambda) d\lambda = hc \int \alpha(E) \frac{dE}{E^2} \cong \frac{hc}{E^2} \int \alpha(E) dE. \quad (4.1)$$

This area was measured with a planimeter. The additive background could be sketched in very accurately at low temperatures where the lines are sharp, and extrapolated from this as the temperature was increased. Line positions at high temperatures where the lines are broad were determined as the point about which the line had equal area on the right and on the left.

The magnetic-field data were taken photometrically with the detector and Jarrel-Ash spectrograph described above. The field was produced by a Lockheed superconducting magnet, whose sample chamber is arranged so that the cooled magnet core can be used as a cold finger to cool the sample. The sample temperature was measured to be about 16°K. Linearly and circularly polarized light was obtained using Polaroid HN22 and HNCP 37 neutral sheet polarizers, respectively, the polarizer being placed between the sample and the spectrometer.

Uniaxial stress was obtained pneumatically by applying a known pressure from a helium gas bottle to a large piston of known area. The piston was on the end of a long stainless-steel rod that extended, inside a stainless-steel guide, down into a large glass helium Dewar, and pressed on the sample. Because very thin samples were used the pressure was applied to the sample's large flat surfaces, and since the light must also be propagated normal to these surfaces, the light was sent into a small hole in the stress rod, reflected down the inside of the rod by a right-angle mirror, passed successively through a small aperture in a copper pad, a transparent sapphire plunger, the sample, a transparent sapphire anvil, and the aperture of another copper pad, and then reflected back out of the system by a final right-angle mirror through a small hole in the stainless-steel base. The sapphire pieces delivered a reasonably uniform stress to the sample. Data were taken photographically on Kodak type 103a-U plates using a Bausch & Lomb 2-m spectrograph in second order, giving a spectral resolution of about 0.5 cm^{-1}. Wavelength calibration was obtained with a neon lamp whose spectrum was slightly superposed on each data trace.

The unpolarized transverse Zeeman spectrum is shown in Fig. 1, and was described in Sec. I. These data confirm that published by van der Ziel,[1] but are of considerably better quality. In Fig. 8 is shown the circularly polarized axial Zeeman spectrum of a flux-grown sample for light propagating along the field direction. Both lines 1 and 4 are polarized in the same way, with the higher and lower energy line of each split pair being, respectively, left and right circularly polarized. As shown in Sec. II, this experimental result constitutes strong evidence that both lines 1 and 4 are indeed transitions to Γ_1 E exciton states.

The shift with temperature of the positions of lines 1–4 was measured from 4°K up to the temperatures where the lines become too broad to be observable, these temperatures being about 220°K for lines 1 and 4, and about 190°K for lines 2 and 3. The shifts, which resemble those measured for the R lines in ruby, are to lower energies as the temperature increases, and are quite large, 20, 21, 30, and 35 cm^{-1} for lines 1, 2, 3, and 4, respectively, at 180°K. These over-all shifts presumably are due to static and dynamic phonon and magnon effects, and probably would be susceptible to an interpretation on this basis. Of central interest to the present discussion, however, is the behavior of the separations of lines 1 and 4, and 2 and 3, because the analysis of Sec. III has shown the principal mechanism for their separations to be the exchange interactions responsible for magnetic ordering and it is expected that as the magnetic order in the crystal is destroyed by thermal fluctuations this mechanism will be less and less effective in producing an energy separation. Therefore the variation with T/T_N of these two separations, normalized to their 4.2°K values, has been plotted in Fig. 9 along

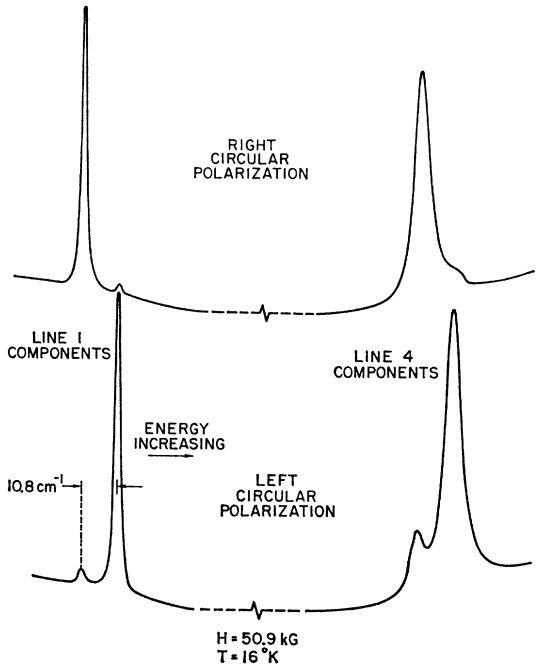

FIG. 8. Circular polarizations of lines 1 and 4 in axial Zeeman experiment.

with the reduced sublattice magnetization deduced for Cr_2O_3 by Hornreich and Shtrikman.[27] Both splittings do indeed collapse rather well with the magnetization, although it is somewhat surprising that the 1–4 separation decreases faster than the magnetization since it seems likely that the separation would depend more on the presence of short-range order, which disappears more slowly than the long-range order which the magnetization measures. In view of the extreme difficulty in locating the positions of the lines at high temperatures where they are very broad, the detailed behavior

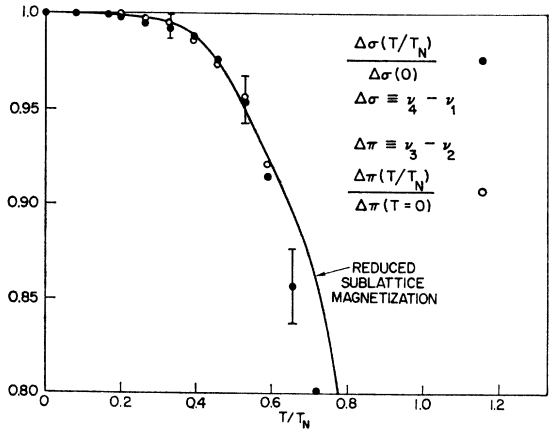

FIG. 9. Temperature dependence of reduced sublattice magnetization and changes of the energy separations of lines 1 and 4, and 2 and 3, normalized to their low-temperature values.

[27] R. Hornreich and S. Shtrikman, Phys. Rev. **161**, 506 (1967).

should not be taken too seriously, however. Rather, the interpretation should be that the splittings follow the magnetization well enough to provide good evidence that the exchange interaction is indeed the correct mechanism.

Figure 10 shows the variation with temperature of the per-ion integrated intensities of lines 1–5 for a vapor-transport-grown sample. The data for other samples are qualitatively the same, although there does appear to be some sample dependence of the 4.2°K intensity of line 5, it being strongest in the flame-fusion samples, and of the 4.2°K relative intensities of lines 1 and 4, these being nearly equal in the vapor-transport and flux-grown samples and in a ratio of about 2 :1, respectively, in the flame-fusion samples. It can be noted that in the model of Sec. II, the intensities of lines 1 and 4 would be equal, again suggesting the effects of some sort of defects in the flame-fusion samples. With the exception of line 1, the low-temperature intensities in Fig. 10 agree fairly well with those given by van der Ziel, which were for a flame-fusion sample. The most striking feature of the data is the increase in intensity of lines 1 and 2 with increasing temperature, since it is usually observed that as a line broadens with increasing temperature, its peak intensity decreases to conserve the area under the line. The increase slows down at about 150°K and it appears that, at least for line 1, a peak occurs at this temperature. The intensities of the other three lines are nominally constant with temperature although there may be some inclination, which is difficult to establish definitely, for them to decrease slightly as the temperature is raised. Unfortunately, no satisfactory explanation of the behavior of lines 1 and 2 is presently available. It can be noted that Nelson and Sturge[28] have reported similar behavior for the R_1 and R_2 lines in ruby, although the increase observed by them was by no more than 30%, while it is found here that line 1 increases its intensity by nearly a factor of 5. Sturge attributed the phenomenon in ruby to a phonon-induced increase in the odd component of trigonal crystal field, which is a part of the chain of perturbation mechanisms required to explain the dipole moment of the $^4A_2 \rightarrow {}^2E$ transition of the Cr^{3+} ion. Whether this mechanism is responsible for the phenomenon in Cr_2O_3 remains an open question. What is required is a careful analysis of the thermodynamics of a magnetic insulator with respect to the optical spectrum, and this does not appear to have been undertaken by anyone at the present time. A past difficulty in doing such an analysis for Cr_2O_3 has been the lack of a consistent low-temperature assignment for the sharp lines in the spectrum. This difficulty, at least, has been remedied by the present work.

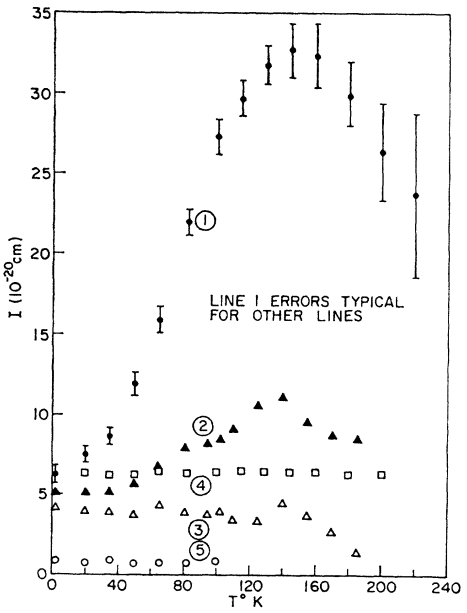

FIG. 10. Temperature dependence of integrated intensities of lines 1–5.

The effect of uniaxial stress applied in the [0001], [11$\bar{2}$0], and [10$\bar{1}$0] directions is to shift lines 1–5 linearly to lower energies by amounts ranging between 0.042 and 0.092 $cm^{-1}/kg\,mm^{-2}$, depending on the stress direction and the line. It was hoped that stress would have a sufficiently profound influence as to produce effects like those obtained by applying a magnetic field, and that, in particular, a transition to the missing A_1^+ level might be induced; however, this is clearly not the case since the uniform shifts observed indicate that the levels do not interact with one another for the magnitude of stress applied, which was as large as 150 kg/mm^2. The over-all shifts are due to changes in single-ion crystal-field parameters and changes in interion interaction parameters, and may be compared with the results of Feher and Sturge[29] on the uniaxial stress dependence of the R lines in ruby, which are observed to shift linearly to lower energies with slopes ranging from 0.017 to 0.026 $cm^{-1}/kg\ mm^{-2}$, depending on the stress direction and the line. The shifts in Cr_2O_3 are in the same direction but somewhat larger, possibly indicating contributions due to interion interactions not present in ruby.

We have been concerned here primarily with single excitations near the center of the Brillouin zone. These have distinct polarization properties since the zone center is a region of high symmetry. Line 5, on the other hand, shows mixed polarization. Its properties suggest that it is a magnon sideband of line 1, i.e., a double excitation involving the lowest ^2E, E excitons, and magnons (also having E symmetry at the center of the zone) throughout the zone. Selection rules allow such a process and in σ and π polarization at all special and general points.In an axial magnetic field, line 5 splits uniformly (see

[28] D. F. Nelson and M. D. Sturge, Phys. Rev. **137**, A1117 (1965).

[29] E. Feher and M. D. Sturge, Phys. Rev. (to be published).

Fig. 1) with a g value of 3.3 ± 0.3. The large uncertainty is due to the initial width and weakness of the line which is compounded when it splits in a field. To a first approximation we would expect a magnon sideband to have a g value equal to $g_{exc}-g_{mag}$ or 2.7. Between 4 and 140°K, beyond which line 5 is too broad to observe, the separation between line 5 and line 1 falls somewhat faster than the sublattice magnetization measured in neutron scattering.[30] In fact, probably coincidentally, it falls like a Brillouin function for spin $\frac{3}{2}$. This difference may arise from the effect of exciton-magnon coupling on the energy renormalization. Zone-boundary magnon energies are not yet known for Cr_2O_3, but we can extrapolate Samuelsen's neutron data[31] out to the zone boundary, and find an energy ≈ 250 cm^{-1}. An exciton-magnon density of states peak (line 5) 227 cm^{-1} from the $k=0$ exciton energy (line 1) is then reasonable. Wickersheim[3] has previously assigned line 5 as a vibronic, but with the additional information that we now have on its properties it appears that his assignment was incorrect.

In summary, this section has presented some new data for lines 1–5, of which the circular polarizations of the magnetically split components of lines 1 and 4 and the temperature shifts of the separations of lines 1 and 4, and 2 and 3, confirm very well the reassignments made in this work. Unfortunately, the temperature-dependent integrated intensities, perhaps the most interesting data, remain unexplained and should be a good topic for future study.

ACKNOWLEDGMENTS

It is a pleasure to acknowledge Catherine A. Allen for her aid in computing the matrix elements in Sec. III, and Robert Griffin for his excellent sample preparation. The furnishing of flame-fusion crystals by R. A. Lefever of the Sandia Corporation, of flux-grown crystals by D. M. Roy of the Pennsylvania State University Materials Research Laboratory, and of vapor-transport-grown crystals by R. C. Folweiler of the Lexington Laboratory is greatly appreciated.

[30] L. M. Corliss and J. M. Hastings, J. Phys. (Paris) **25**, 557 (1964).
[31] E. J. Samuelsen, Phys. Letters **26A**, 160 (1968).

PHYSICAL REVIEW VOLUME 179, NUMBER 2 10 MARCH 1969

Direct Measurements of Anisotropy Energy and Anisotropic Magnetization in Gallium Iron Oxide

JOHN H. SCHELLENG AND GEORGE T. RADO
Naval Research Laboratory, Washington, D. C. 20390
(Received 28 October 1968)

Direct measurements are reported of the dependence of the anisotropy torque on the orientation of an applied magnetic field in the *ac* and *bc* crystallographic planes of ferrimagnetic $Fe_xGa_{2-x}O_3$ for $x=1.11$. Temperatures between 4.2 and 294°K and applied fields up to 110 kOe were used. Anisotropic spontaneous magnetizations, as well as isotropic susceptibilities and field-dependent anisotropy energies, were determined by comparing the experimental data with a new thermodynamic analysis of the magnetic properties of spontaneously magnetized orthorhombic crystals. The larger of the values obtained at 4.2°K for the zero-field anisotropy energy (3.22×10^6 erg/cm^3 and 5.65×10^6 erg/cm^3 in the *ac* and *bc* planes, respectively) is the largest value of this quantity measured so far in any insulator. The contributions of classical dipolar interactions to the zero-field anisotropy energy at 0°K are calculated to be 1.22×10^6 and 4.19×10^6 erg/cm^3 in the *ac* and *bc* planes, respectively. The remainder of the anisotropy energy is shown to be probably due to one-ion anisotropy or antisymmetric exchange or both. The largest values obtained for the fractional anisotropy of the spontaneous magnetization (0.24 and 0.55 in the *ac* and *bc* planes, respectively, at 294°K) are, to our knowledge, the largest values of this quantity measured so far in any material. It is found, moreover, that the anisotropic part of the spontaneous magnetization does not tend to zero as the temperature approaches 0°K. Direct measurements of the anisotropic magnetization are reported for 276 and 294°K, and the results are found to agree satisfactorily with those deduced from the torque measurements.

I. INTRODUCTION

GALLIUM iron oxide, $Fe_xGa_{2-x}O_3$ (where $0.7<x<1.4$), was first synthesized by Remeika,[1,1a] who found it to be both ferromagnetic and piezoelectric. In 1964 Rado[2] reported that it is the first ferromagnetic material known to exhibit the magnetoelectric effect. Other authors have studied its spontaneous moment and susceptibility,[3,4] its crystallographic structure,[5,6] its

[1] J. P. Remeika, J. Appl. Phys. **31**, 263S (1960).
[1a] A brief report on that part of this work which deals with the anisotropic spontaneous magnetization was published in Phys. Letters **A28**, 318 (1968).
[2] G. T. Rado, Phys. Rev. Letters **13**, 335 (1964); in *Proceedings of the International Conference on Magnetism, Nottingham, 1964* (The Institute of Physics and The Physical Society, London, 1965), p. 361; J. Appl. Phys. **37**, 1403 (1966).
[3] C. Nowlin and R. V. Jones, J. Appl. Phys. **34**, 1262 (1962).
[4] A. Pinto, J. Appl. Phys. **37**, 4372 (1966).
[5] S. C. Abrahams and J. M. Reddy, Phys. Rev. Letters **13**, 688 (1964); S. C. Abrahams, J. M. Reddy, and J. L. Bernstein, J. Chem. Phys. **42**, 3957 (1965).
[6] E. F. Bertaut, G. Buisson, J. Chappert, and G. Bassi, Compt. Rend. **260**, 3355 (1965).